Splitter-Bladed Centrifugal Compressor Impeller Designed For Automotive Gas Turbine Application

by R. C. Pampreen

CHRYSLER CORPORATION

prepared for
National
Aeronautics
and
Space
Administration

NASA
National Aeronautics and Space Administration

Lewis Research Center
Cleveland, Ohio 44135
AC 216 433-4000

Contract
NAS 3-20059

1. Report No.	2. Government Accession No.	3. Recipient's Catalog No.
NASA CR-135237		

4. Title and Subtitle	5. Report Date
SPLITTER-BLADED CENTRIFUGAL COMPRESSOR IMPELLER DESIGNED FOR AUTOMOTIVE GAS TURBINE APPLICATION	June 1977
	6. Performing Organization Code

7. Author(s)	8. Performing Organization Report No.
R. C. Pampreen	
	10. Work Unit No.

9. Performing Organization Name and Address	11. Contract or Grant No.
CHRYSLER CORPORATION Highland Park, Michigan	NAS 3-20059
	13. Type of Report and Period Covered

12. Sponsoring Agency Name and Address	13. Type of Report and Period Covered
NATIONAL AERONAUTICS AND SPACE ADMINISTRATION Cleveland, Ohio	Contractor Report
	14. Sponsoring Agency Code

15. Supplementary Notes

Project Manager, Lawrence F. Schumann, Lewis Directorate, USAAMRDL, Cleveland, Ohio

16. Abstract

Mechanical design and fabrication of two splitter-bladed centrifugal compressor impellers were completed for rig testing at NASA Lewis Research Center. These impellers were designed by NASA for automotive gas turbine application. The mechanical design was based on NASA specifications for blade-shape and flowpath configurations. The contractor made engineering drawings and performed calculations for mass and center-of-gravity, for stress and vibration analyses, and for shaft critical speed analysis. One impeller was machined to print; the other had a blade height and exit radius of 2.54 mm larger than print dimensions.

17. Key Words (Suggested by Author(s))	18. Distribution Statement
Compressor, Impeller	Unclassified - Unlimited

19. Security Classif. (of this report)	20. Security Classif. (of this page)	21. No. of Pages	22. Price*
UNCLASSIFIED	UNCLASSIFIED		

* For sale by the National Technical Information Service, Springfield, Virginia 22161

Foreword

This is the final report covering work performed by Chrysler Corporation under Contract No. NAS 3-20059 during the period 1 September 1976 to 30 June 1977. The Project Manager was Mr. L. F. Schumann, Lewis Directorate of the U.S. Army Air Mobility Research and Development Laboratory. Chrysler participation was under the direction of Mr. C. E. Wagner, Program Manager, and Mr. R. C. Pampreen, Principal Engineer. Recognition is also given to F. Dosenberger, Mechanical Design, and D. S. Musgrave, Aerodynamics, of Chrysler Corporation, for their special skill contributions.

Table of Contents

SUMMARY 1

INTRODUCTION 1

BLADE COORDINATE DEFINITION 2

MASS AND CENTER-OF-GRAVITY CALCULATIONS 8

STRESS ANALYSIS 8

BLADE VIBRATION ANALYSIS 9

CRITICAL SPEED ANALYSIS 9

CONCLUSION 12

Summary

Mechanical design and manufacture of two splitter-bladed centrifugal compressor impellers was completed for rig testing at NASA Lewis Research Center. The full-blade geometry is similar to that of an impeller previously designed for the ERDA Automotive Gas Turbine Program (Contract No. E(11-1)-2749). This reference impeller was designed without splitters and had high aerodynamic loading on the rear half of the blade. To minimize inertia and engine acceleration time the addition of splitters was considered a means of improving rotor efficiency through reduction of blade loading. The blade angle distribution of the splitter was identical to the corresponding positions on the full blade except for the leading edge. The NASA specification of splitter leading-edge angle distribution was based on matching the local channel flow direction between the full blades. Since the addition of the splitters was expected to increase compressor work, the tip diameter was reduced by an amount determined from a calculated estimate of work coefficient.

The contractor computed the blade coordinates for this design for blueprint definition. Calculations were performed for mass and center-of-gravity, for stress and vibration analyses, and for shaft critical speed analysis. The contractor made engineering drawings and procured two impellers. One impeller was machined to print; the other had a blade height and exit radius of 2.54 mm larger than print dimensions.

Introduction

The Energy Research and Development Agency (ERDA) is conducting a program to demonstrate a gas turbine powered automobile that meets Federal Emissions Standards with acceleration characteristics and fuel economy that are competitive with current conventionally powered vehicles. As part of this program, a 75 KW upgraded engine for a 1600 Kg vehicle is being designed and built by the Chrysler Corp. The turbomachinery components for this engine were designed by the NASA Lewis Research Center. The design results are described in References 1-3.

Because of the cyclic nature of the duty cycle for automotive power plants, the moment of inertia of the rotating components has an important effect on the fuel economy of the engine operating on a given driving cycle. Thus some component efficiency can be sacrificed to reduce inertia or increase engine response and still achieve an improvement in driving cycle fuel economy. The original compressor for the upgraded engine had an impeller with 18 backswept blades and a short axial length. Both of these characteristics represent compromises for improved driving cycle fuel economy. The backswept impeller has efficiency and flow range characteristics that are superior to a radial bladed design. As a compromise to low inertia, the 18-blade design has rather high aerodynamic loading near the impeller exit. In an effort to bias the compromise to higher efficiency, impellers with 24 blades and 18 blades and 18 splitters were designed. The 24-blade design had blades that were identical to the original 18-blade design. Experimental evaluation of the two designs at NASA showed no appreciable difference in efficiency. Preliminary design analysis shows that there should be an improvement in efficiency with the 18-18 design. This report discusses the method of blade shape coordinate definition and the mechanical design analyses that were carried out for the 18-18 design.

BLADE COORDINATE DEFINITION

Calculation Method

In order to understand the work necessary to translate the given impeller geometrical description into drawings for machining definition (or a computer tape for use by a 5-axis machine tool), it is necessary to understand the method of calculation in the computer program which was used for this purpose. A brief description is given below.

The computer program defines a mean camber surface from specified values of blade angles at the hub and shroud. The computed geometrical parameters are compared with the design geometrical parameters for computational consistency as explained below. Specified values of normal thickness are added to the camber surfaces at defined locations. All terms are defined in the Nomenclature Section. Dimensional coordinates, (R,Z) are given for two lines in meridional space - the hub contour and the shroud contour. The blade angle, β, is supplied along these lines as a fraction of dimensionless distance. The normalizing distances used at the hub and shroud were determined from the calculation stations shown in Fig. 1. The polar angle, θ, is then determined by a finite difference integration along each of two lines.

The polar angles, θ, for the hub and shroud are used with a machine tool angle, ψ, to determine intermediate values of θ for other lines (or points) on the blade. The machine tool is assumed to be straight; hence, a linear distribution of θ exists along the tool axis from hub to shroud points of intersection. The selection of ψ will thus determine the values of θ (and β) at intermediate points.

Finally, a normal thickness specified along the hub and shroud is used to determine intermediate normal thicknesses by also using a linear variation along the machine tool axis. Tangential thicknesses and other sections of the blade geometry can then be obtained by using local values of the various angles, their components and the normal thickness.

The required information of Z, R, β and normal thickness along the hub and shroud lines was supplied by NASA. Additionally, the meridional distance of the polar angle θ was supplied for the above points. An interpolation scheme was used to create intermediate points between each specified pair. The specified and interpolated points were then used to compute the line integral for the hub and shroud contours. The computed meridional distances were compared with the supplied values to confirm that the curve-fitting technique and the number of points used in the input had accurately generated the desired hub and shroud coordinates.

The blade angle β on a streamline is related to the polar angle, θ, and the meridional distance, m, by

$$\text{Tan}\,\beta = \frac{R\,d\theta}{dm}$$

The specified values of β are used to determine the variation of θ with m. The values of θ are used to compute the cylindral blade angle, β^*, and the lean angle, ϵ. These angles are then used to recompute the input values of β to check errors in numerical differentiation.

The mean streamline properties that were supplied allow selecting a machine tool angle (ψ) distribution to achieve the desired intermediate properties.

Hub- and Shrould-Line Definition

The impeller has hub and shroud meridional coordinates identical to that of a previously designed 18-blade impeller with the exception of the tip radius, which has been reduced (see Figure 1). The given Z-value of the shroud tip was adjusted slightly (from 30.48 mm to 30.38 mm) so that the same impeller cover can be used. The meridional contours were extended at both the leading edge and trailing edge to allow for the creation of extrapolated sections. All the points were then used in the program to create 7 intermediate points between each specified pair through use of a second-order Forsythe polynomial. The resulting points were used to evaluate the previously mentioned line integrals for each contour. A comparison of computed distances with the meridional distances supplied is shown in Table I. Agreement is very good (maximum error is about 0.05 mm) indicating that the curve-fitting technique and increment size have accurately generated the desired hub and shroud coordinates.

TABLE I

Comparison of Specified and Computed Meridional Distances

	Given on the Hub:			**Calc. M**	**Error**
	Z(mm)	R (mm)	M (mm)	M (mm)	(mm)
L.E.	3.05	25.40	0.	0.	0.
	10.58	27.61	7.85	7.85	0.
	16.46	30.60	14.45	14.45	0.
	25.24	38.10	25.99	26.02	.03
	30.85	46.79	36.33	36.38	.05
	33.68	55.70	45.69	45.73	.04
	34.32	64.31	54.32	54.37	.05
	34.47	73.33	63.34	63.39	.05
T.E.	34.47	80.62	70.63	70.68	.05
	Given on the Shroud:			**Calc. M**	**Error**
	Z (mm)	R (mm)	M (mm)	M (mm)	(mm)
L.E.	3.05	44.71	0.	0.	0.
	7.89	44.99	4.85	4.86	.01
	12.22	45.72	9.24	9.25	.01
	18.11	48.19	15.62	15.64	.02
	22.74	51.97	21.60	21.63	.03
	26.49	57.70	28.45	28.49	.04
	28.83	65.11	36.22	36.27	.05
	30.05	73.49	44.69	44.74	.05
T.E.	30.38	80.62	51.83	51.88	.05

Full-Blade Geometry

The impeller design uses 18 full blades and 18 splitter blades. The splitters are not full blades that have been cut back, but are instead a slightly different geometry. Thus, two complete geometrical descriptions were necessary. The full blades will be considered first.

With the meridional distances along the hub- and shroud-lines known, a normalized table of the given blade angle, β , and normal thickness along each line can be created. Figures 2 and 3 show the resulting β-distributions, including those of the original 18-blade impeller. In both

cases, the circular points were supplied, and the plus points were added. These latter adjustments were defined by French-curve definition in order to extend the flowpath extrapolating sections or to help generate the correct polar angle at the input points.

The program has an internal self-consistency check to see if the components of β (β^*, the cylindrical blade angle and ϵ, the lean angle) are being computed correctly from numerical derivatives. These angles are used in calculating the tangential thickness of any point. The values of β^* and ϵ, along with the local slope, α, are used to recompute β at the input points. A comparison with the input β versus the calculated β reflects the errors in numerical differentiation and in the determination of the local "streamline" slope. The polar angle, θ, is also displayed.

Table 2 displays the Z,R coordinate pairs supplied for the hub and their values of β and θ. Also shown are the errors resulting from the calculated values of β (from β^* and ϵ) and θ (from input values of β) plus the values of β^*, ϵ and α used in the calculations.

TABLE 2 (HUB)
Comparison Of Specified β And θ On HUB With Computed Values
All Angles In Degrees, Program Values In ( )

Z (mm)	R (mm)	BETA	(BETA ERROR)	THETA	(THETA ERROR)	(β^*)	(ϵ)	(α)
3.05	25.40	53.72	.37	26.50	0.	−54.07	10.16	14.47
10.58	27.61	41.46	.43	45.69	−.09	−43.14	3.42	20.90
16.46	30.60	28.33	.32	54.87	.11	−33.52	−1.05	32.89
25 24	38.10	11.93	−.13	61.69	.00	−19.81	−1.59	50.29
30.85	46.79	9.64	1.66	64.20	.04	−15.01	6.35	69.03
33.68	55.70	12.34	−.26	66.22	.02	−5.31	11.64	84.45
34.32	64.31	16.81	.05	68.32	.05	.35	16.87	88.86
34.47	73.33	24.44	−.10	71.11	.06	2.35	24.34	90.00
34.47	80.62	30.20	−.11	73.94	.02	1.57	30.09	90.00

With the exception of one point (#5), the β-errors are well under one degree. The main reason for the larger error (1.662 degrees) at point #5 is the difficulty of determining the local slope in this region of highest flowpath curvature. An increase in α of only 5 degrees would cut the error to 0.6 degree. The value of α could easily change by 5 degrees depending on the curve-fitting technique employed. Since α is not used during the calculation of point properties, errors in this region should be no larger than elsewhere. The errors in polar angle θ are of the order of 0.1 degree and primarily indicate the way in which the β-curve is drawn. The plus marks on Figures 2 and 3 reflect effort to match the desired θ-values by refinements in the β distribution.

Figure 4 shows the normal thickness distribution on the hub. The shroud has a constant value of 0.508 mm. Since the normal thicknesses do not depend on integrals or derivatives along the flowpath lines, the output values are identical to the input values.

Table 3 presents the calculation results for the shroudline. Virtually all of the same comments apply, including the slope ambiguity in the region of maximum curvature.

TABLE 3 (SHROUD)

Comparison Of Specified β And θ On Shroud With Computed Values All Angles In Degrees, Program Values In ( )

Z (mm)	R (mm)	BETA	(BETA ERROR)	THETA	(THETA ERROR)	(β^*)	(ϵ)	(α)
3.05	44.71	61.96	.16	33.61	−.10	−62.09	14.59	.60
7.89	44.99	54.05	.27	43.70	−.08	−54.14	8.92	6.68
12.22	45.72	44.93	.36	50.25	−.01	−45.63	4.31	13.92
18.11	48.19	34.04	.20	56.59	−.01	−37.53	2.78	31.45
22.74	51.97	28.60	.01	60.76	−.01	−34.30	7.02	48.34
26.49	57.70	25.28	−.97	64.35	.02	−29.44	14.71	68.43
28.83	65.11	24.70	−.55	67.73	.01	−21.49	21.06	79.88
30.05	73.49	26.80	−.16	71.04	.05	−9.12	26.24	86.57
30.38	80.62	30.20	−.05	73.94	.02	−2.41	30.13	89.17

The work described so far completely specifies all properties along the hub and shroud lines. The interior region, however, is not defined until a definite machine-tool cutter-angle distribution is selected. For the first run, it was decided to use the distribution of the original 18-blade design, check the errors, and then make adjustments. The results, shown in Table 4 reveal errors in β and θ that are no larger than those on the hub and shroud.

TABLE 4 (MEAN)

Comparison Of Specified β And θ On Meanline With Computed Values All Angles In Degrees, Program Values In ( )

Z (mm)	R (mm)	BETA	(BETA ERROR)	THETA	(THETA ERROR)	(β^*)	(ϵ)	(α)
3.05	35.05	59.01	−.17	30.20	−.03	−58.84	12.46	16.10
9.11	37.12	48.55	.40	44.40	−.08	−49.92	6.55	21.38
14.05	39.26	38.28	−.21	52.08	.00	−40.61	1.94	26.33
21.28	43.49	24.50	−1.08	59.17	−.10	−29.85	.67	42.17
26.55	49.50	18.37	−.87	62.92	−.03	−23.95	6.13	59.99
29.96	56.72	17.86	−.65	65.73	−.01	−17.74	13.31	75.35
31.67	64.71	19.29	.18	68.29	.02	−9.14	18.78	84.63
32.34	73.43	24.60	.20	71.15	.07	−1.60	24.79	88.90
32.46	80.62	30.20	−.36	73.94	.05	.25	29.85	89.03

An additional problem is the interior thickness values. The hub and shroud normal thicknesses were input and hence were exact on output. The interior values, however, depend on an interpolation which involves the local cutter angle value and thus could be in error. Table 5 lists the given values and the program errors. All the errors except the last one are less than 0.025 mm. The last point was deemed acceptable (the error is 5.5%), and thus the blade was completely defined. The original machine-tool cutter-angle distribution was therefore retained for the full blade and a difficult adjustment procedure avoided.

TABLE 5

Table Of Specified Normal Thickness On Mean Streamline With Computed Thickness Error From Specified Value

Z (mm)	R (mm)	Norm. Thick. (mm)	(Thick. Error mm)
3.05	35.05	0.93	0.00
9.11	37.12	0.97	0.00
14.05	39.26	1.02	−0.02
21.28	43.49	1.11	−0.02
26.55	49.50	1.16	−0.02
29.96	56.72	1.17	−0.02
31.67	64.71	1.13	−0.01
32.34	73.43	1.04	0.00
32.46	80.62	0.88	.05

Splitter Blade Geometry

The splitter retains the meridional coordinates and thickness distribution of the full blades. It was also found that the same shroudline β-distribution could be used, and it is presented in Figure 5 with the leading-edge position indicated. Table 6 contains the shroudline errors which result from the calculations. They are of the same order as those for the full blade.

TABLE 6 (Splitter Shroud, Mean, and Hub)
Comparison Of Specified β And θ With Computed Values
All Angles In Degrees, Computed Values In ( )

	Z (mm)	R (mm)	BETA	(BETA ERROR)	THETA	(THETA ERROR)	(β^*)	(ϵ)	(α)
SHROUD	17.56	47.87	34.73	.03	66.10	−.06	−36.91	4.97	30.0
	28.83	65.11	24.70	− .55	77.73	−.01	−21.50	21.06	79.88
	30.05	73.49	26.80	−.16	81.04	.02	−9.12	26.24	86.57
	30.38	80.62	30.20	−.05	83.94	.00	−2.41	30.13	89.17
MEAN	17.56	42.19	31.35	−.29	65.48	.05	−34.33	3.32	33.35
	30.27	58.63	18.46	−1.17	76.33	−.06	−16.03	14.54	78.57
	31.71	66.39	20.19	.16	78.83	−.02	−7.69	19.80	84.63
	32.35	74.70	25.76	−.11	81.64	.02	−1.00	25.67	88.77
	32.47	80.62	30.20	−.36	83.94	.02	.26	29.85	88.92
HUB	17.56	31.34	25.78	.60	64.86	.00	−30.46	1.38	34.94
	30.85	46.79	9.64	1.73	74.20	.01	−15.10	6.39	69.03
	33.68	55.70	12.34	−.26	76.22	.00	−5.31	11.64	84.45
	34.32	64.31	16.81	.05	78.32	.03	.35	16.87	88.86
	34.47	73.34	24.44	−.10	81.11	.04	2.35	24.34	90.00
	34.47	80.62	30.20	−.11	83.94	.00	1.57	30.09	90.00

As Figure 6 shows, the β-distribution on the hub is significantly different from that used for the full blade. The result is that, at the hub, the splitter is biased toward the suction surface of the full blade, along the initial portion of the splitter. The β and θ errors are given in Table 6. The β error of 1.73 degrees is attributed to streamline slope ambiguity.

The use of the full-blade cutter-tool ψ-distribution generated the β and θ errors given in Table 6. They are considered acceptable. Thus, the only major difference between the geometry of the full blade and splitter is the hub β-distribution. The lower β-values over the initial portion of the blade produce the desired θ-angles along the hub. The resulting interior point properties are as specified.

Photographs of the final impeller are shown in Fig. 7.

MASS AND C.G. CALCULATIONS

Figure 8 shows the areas into which an impeller is subdivided in order to compute mass, center-of-gravity and polar moment of inertia in a coded computer program. Table 7 shows the results of the calculations and includes a breakdown of the contributions to inertia for the various areas.

TABLE 7

Summary Of Mass And C.G. Calculations For Splitter-Bladed Impeller

Mass, Kg	1.120
C.G., mm, Relative to Z=0	8.66
Inertia, gm-m^2	2.5090
Inertia Breakdown:	
Body	0.9442
Hole	−0.0165
Disc	0.4363
Ramp	0.6816
Full Blades	0.2706
Splitter Blades	0.1927

STRESS ANALYSIS

This section presents the results of the centrifugal stress and deflection analysis of the compressor disc and blade and an estimate of the impeller burst speed for an assumed average disc operating material temperature.

The stress analysis, which is based on the finite-element approach, was performed to determine an impeller configuration which is capable of withstanding the centrifugal stress environment present in the test rig.

Since the NASA impeller is very much similar to the original proven test-rig impeller (with the exception that it has 18 splitter blades in addition to the 18 full blades), a similar disc profile was selected for the analysis and is shown in Figure 9. The approach taken was to model the impeller based on 36 full blades instead of 18 splitters and 18 full blades. As a result, only a sector, 1/36 of the disc, needed to be analyzed. This reduced considerably the amount of manual input and computer costs. The calculated disc stresses will also be conservative.

The impeller is machined from aluminum alloy 2618-T61 material and is designed to operate for a design speed of 46,475 rpm. The maximum tangential stress occurs at the bore and is equal to 238 MPa. These values are well within the material's yield strength. The disc average

tangential stress is 105 MPa. Based on this value and a burst factor of 0.75, the calculated burst speed is 72,800 rpm; i.e.,

$$\text{Burst Margin} = \sqrt{\frac{0.75 \times \sigma \text{ Ultimate}}{\sigma \text{ Avg. Tang.}}}$$

The burst margin is equal to 1.57.

The finite element model of the impeller, the deformed shape and the stress isoplots for the disc and blades are shown in Figures 9 through 24. The maximum blade principal stress is 132 MPa in tension and occurs at the blade shroudline (suction side) as shown in Figure 19. The equivalent stress is 126 MPa. The centrifugal deflection of the tip is 0.011 mm forward and 0.086 mm outward. These values compare favorably with 0.030 mm forward and 0.083 mm outward deflections for the 18-blade impeller. Since the deflections are reasonably compatible, the consideration of 36 blades for the stress model is fully justified.

BLADE VIBRATION ANALYSIS

The blade frequencies were calculated with the NASTRAN finite element program, using element differential stiffness techniques to adjust the frequencies for the rotational speed. Figure 25 shows that there are no resonance conditions within the anticipated operating range. The first four mode shapes for the blade are shown in Figures 26 through 29.

CRITICAL SPEED ANALYSIS

Since the bearing shaft system of the NASA compressor test rig is identical to the proven Chrysler Baseline Engine system with the exception of the impeller, no analytical dynamic analysis needed to be performed. Two Chrysler impellers, having inertia, mass, and bearing overhang values as shown in Table 8 have been extensively tested with the shaft system used for the NASA rig, and the maximum measured deflection throughout the operating range was measured to be only 0.0254 mm. Table 8 shows the NASA impeller characteristic values to be almost identical to those of the scaled Upgraded Engine impeller. Thus no critical speed problems are anticipated for the NASA test rig.

TABLE 8

IMPELLER	MASS (Kg)	INERTIA (gm-m²)	BEARING OVERHANG (mm)
Chrysler Research Impelier	1.42	3.515	26.5
Upgraded Engine 1.26-Scale (18 Blades)	1.09	2.419	26.8
NASA (18 Blades, 18 Splitters)	1.12	2.509	27.00
Upgraded Engine 1.26-Scale (24 Blades)	1.11	2.502	26.8

Concluding Remarks

Two splitter-bladed centrifugal compressor impellers were procured for rig testing at NASA Lewis Research Center. Chrysler Corporation provided mechanical design services in which blade coordinates were defined for engineering drawings and calculations were performed for structural integrity.

Nomenclature

β - Blade angle; = TAN^{-1} (Rdθ/dm), deg.

θ - Polar angle about axis of rotation, deg.

β^* - Cylindrical blade angle; = TAN^{-1} (Rdθ/dz), deg.

ϵ - Blade lean angle; = TAN^{-1} Rdθ/dR), deg.

R - Radius, mm

Z - Axial distance, mm

M - Meridional distance, mm

ψ - Machine cutter angle, deg.

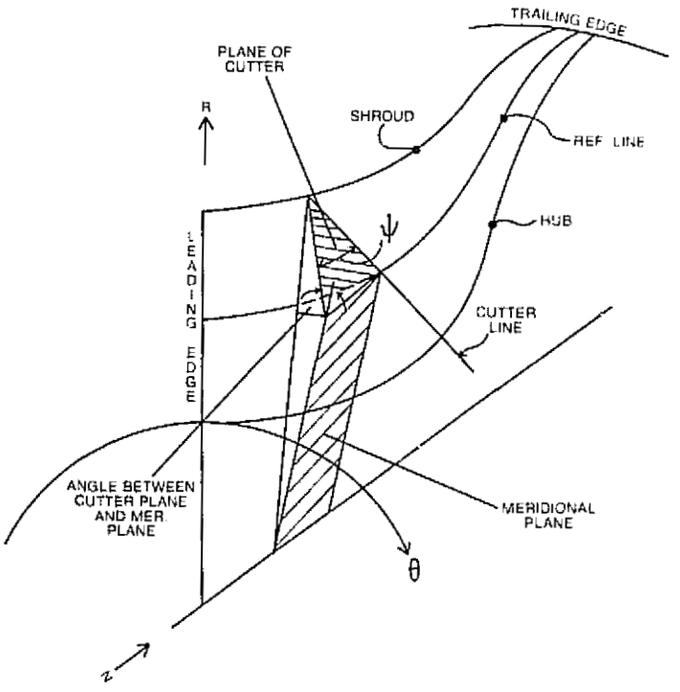

Definition of Cutter Angle

References

1. Galvas, Michael R.: "A Compressor Designed for the Energy Research and Development Agency Automotive Gas Turbine Program". NASA TM X-71719, 1975.

2. Roelke, Richard J. and McLallin, Kerry L.: "The Aerodynamic Design of a Compressor-Drive Turbine for Use in a 75-KW Automotive Engine". NASA TM X-71717, 1975.

3. Kofskey, Milton G., Katsanis, Theodore and Schumann, Lawrence F.: "Aerodynamic Design of a Free Power Turbine for a 75-KW Gas Turbine Automotive Engine". NASA TM X-71714, 1975.

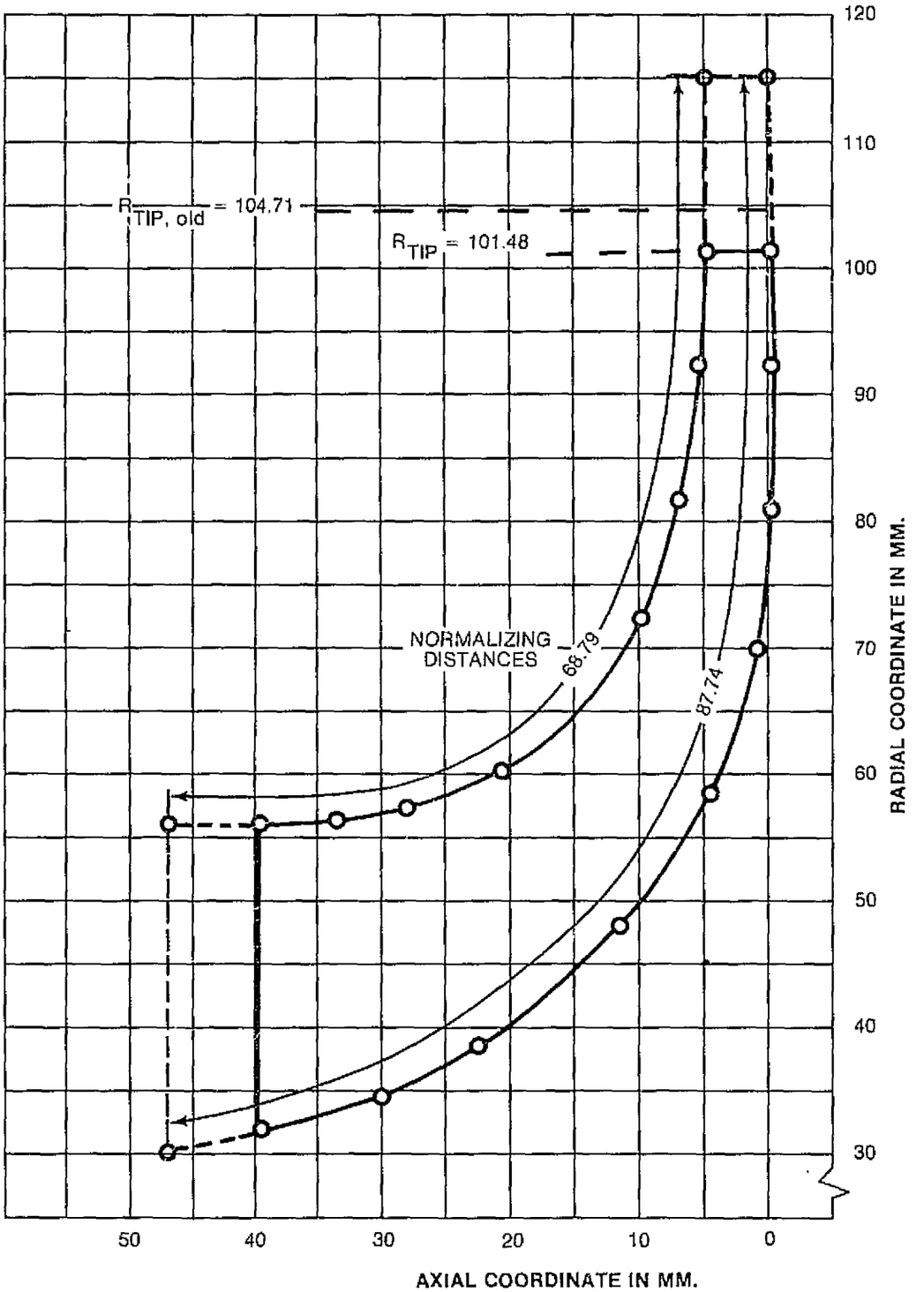

Figure 1
Meridional View Of Impeller
1.2588 Scale

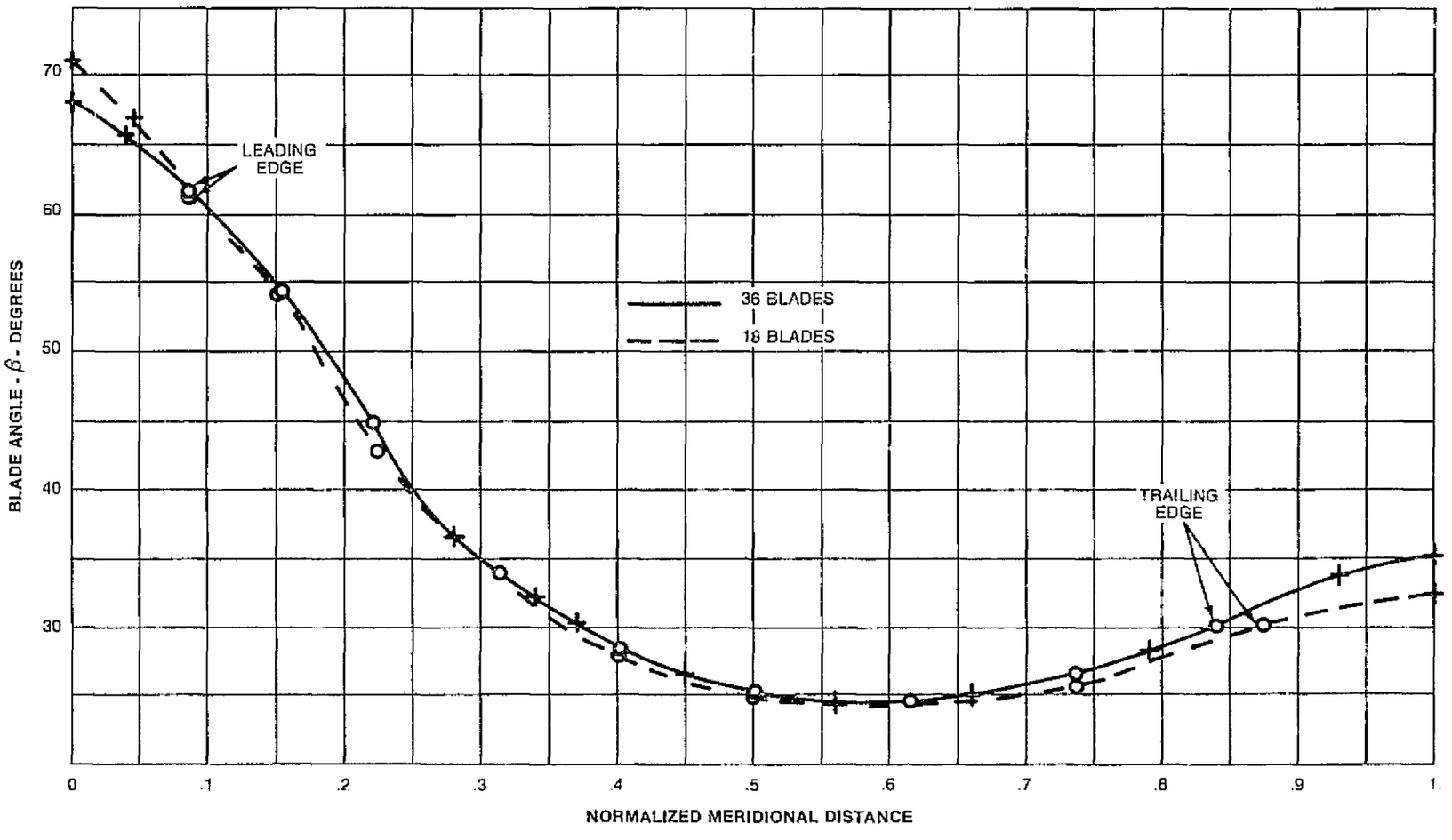

Figure 2
Shroudline Blade Angle Distribution, 36-Blade and 18-Blade Impellers

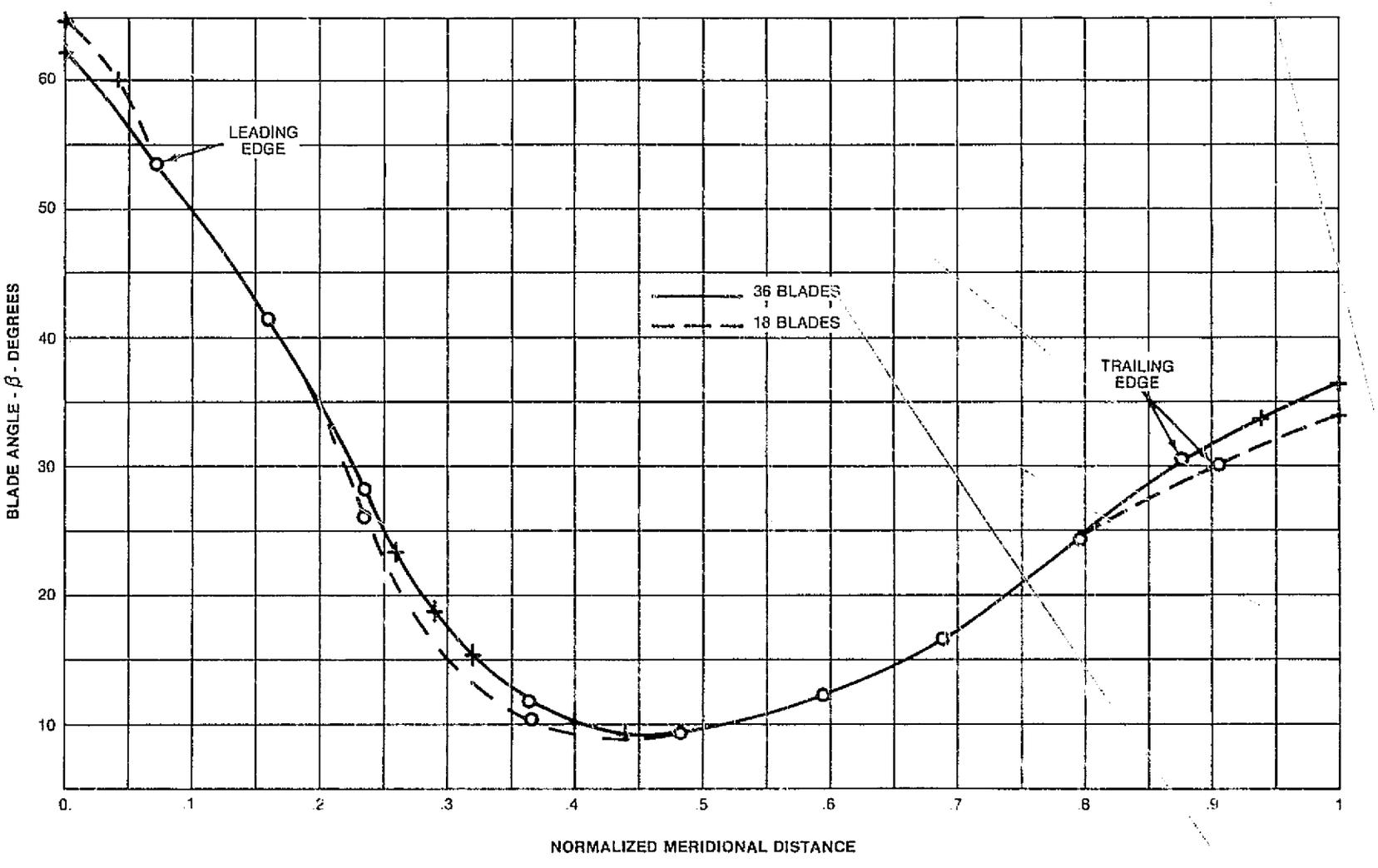

Figure 3
Hubline Blade Angle Distribution, 36-Blade and 18-Blade Impellers

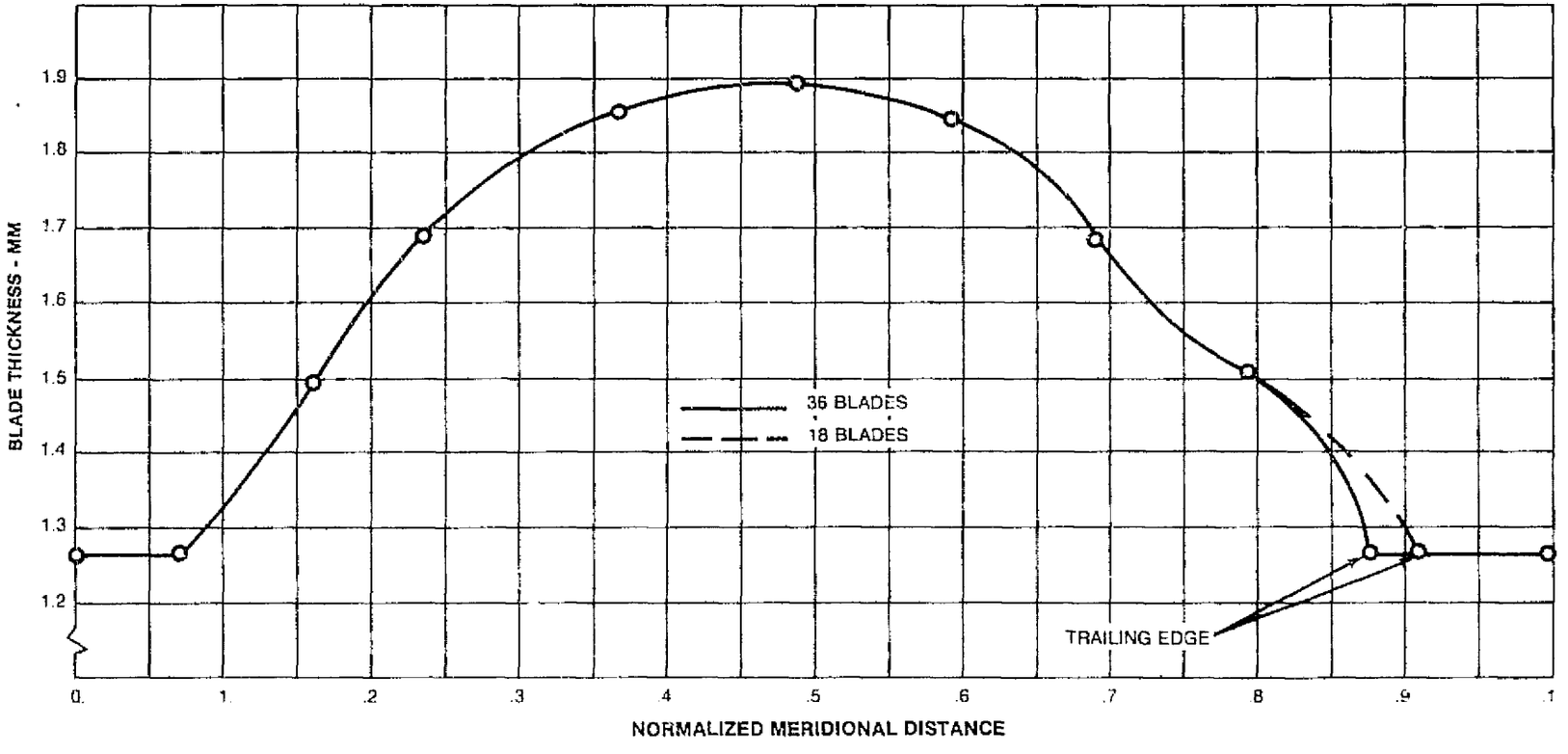

Figure 4
Normalized Thickness Distribution On Hub

NORMALIZED MERIDIONAL DISTANCE

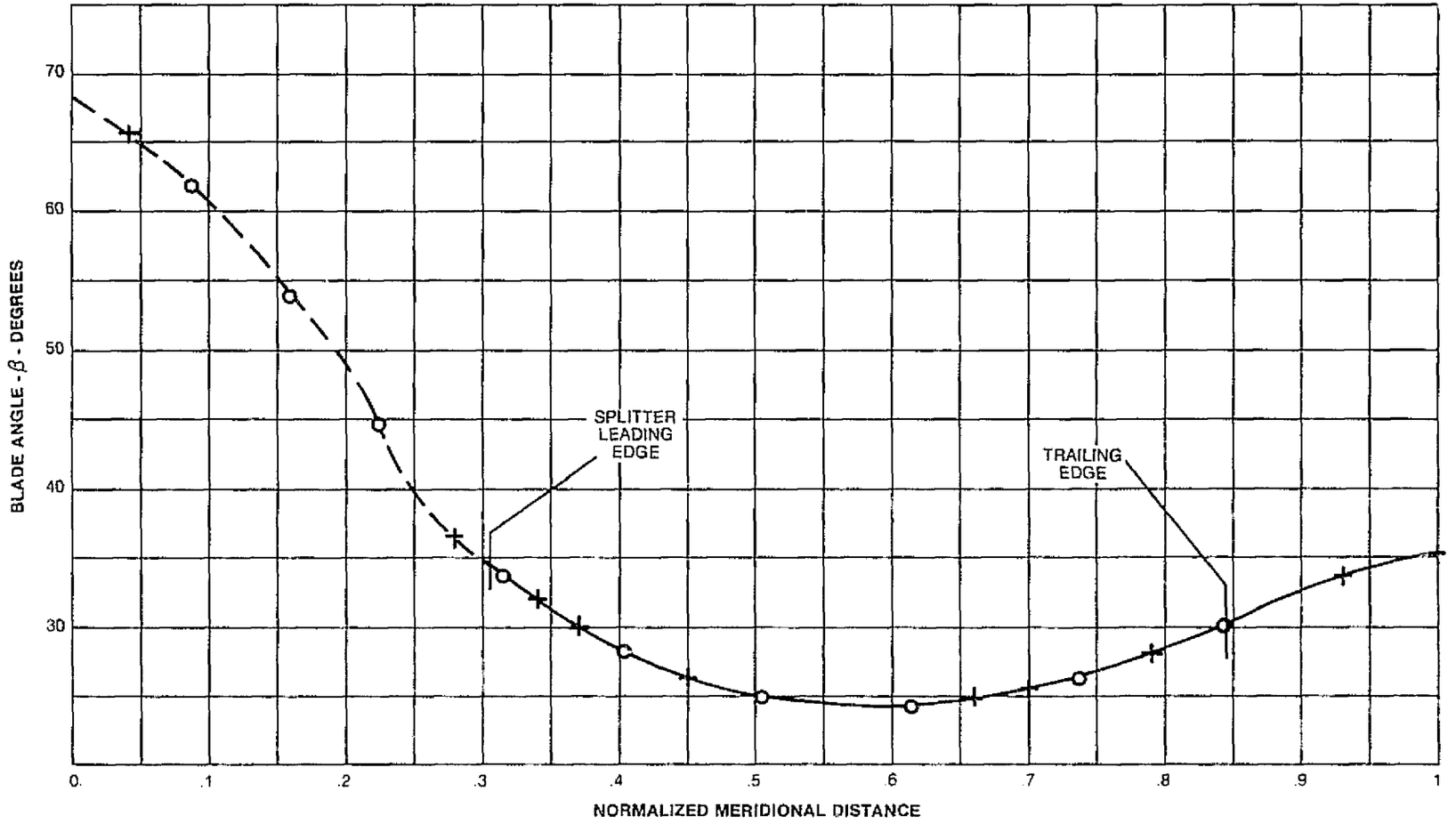

Figure 5
Shroudline Blade Angle Distribution For Splitter Blades (Same As Full Blades)

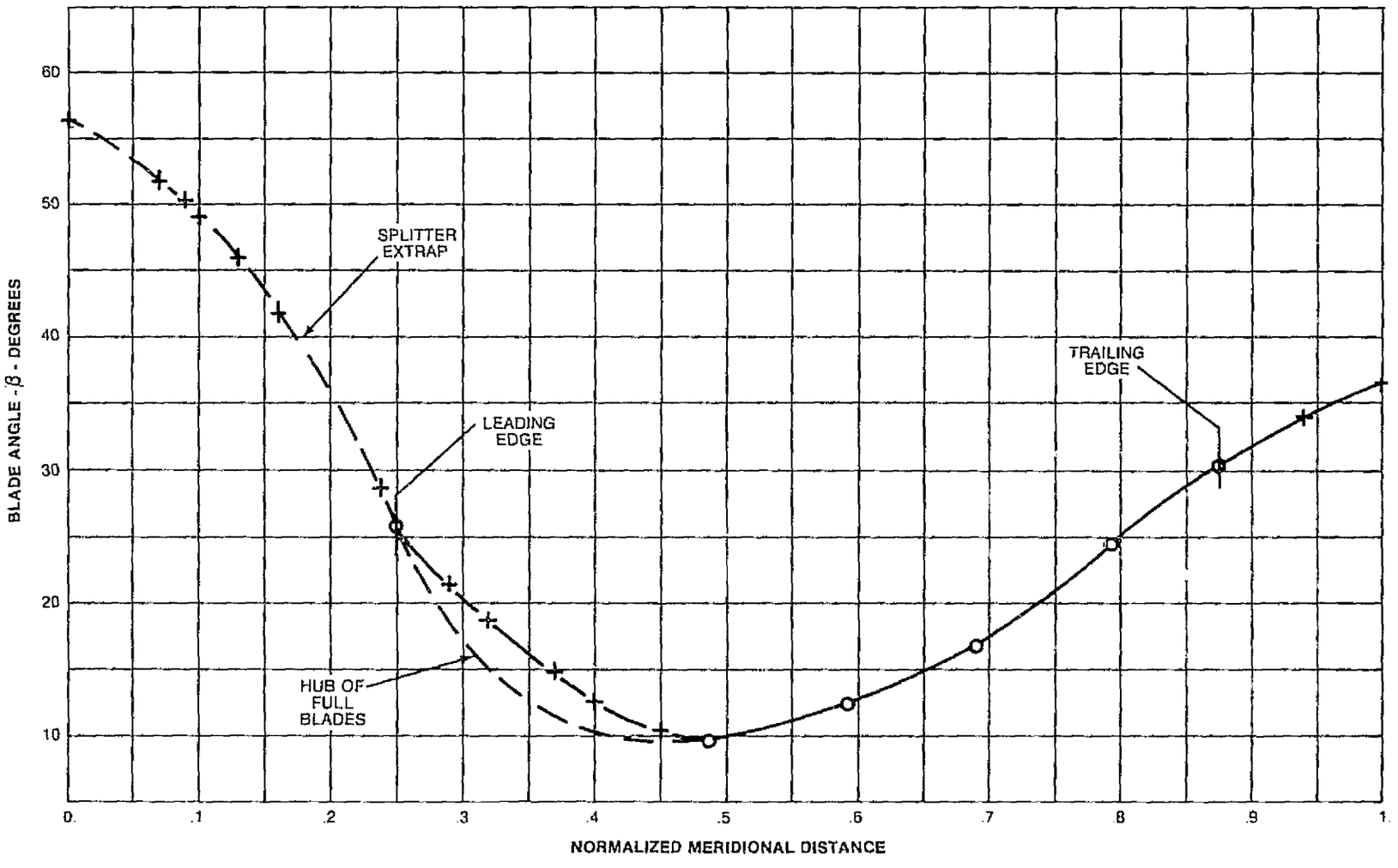

Figure 6
Hubline Blade Angle Distribution For Splitter Blades

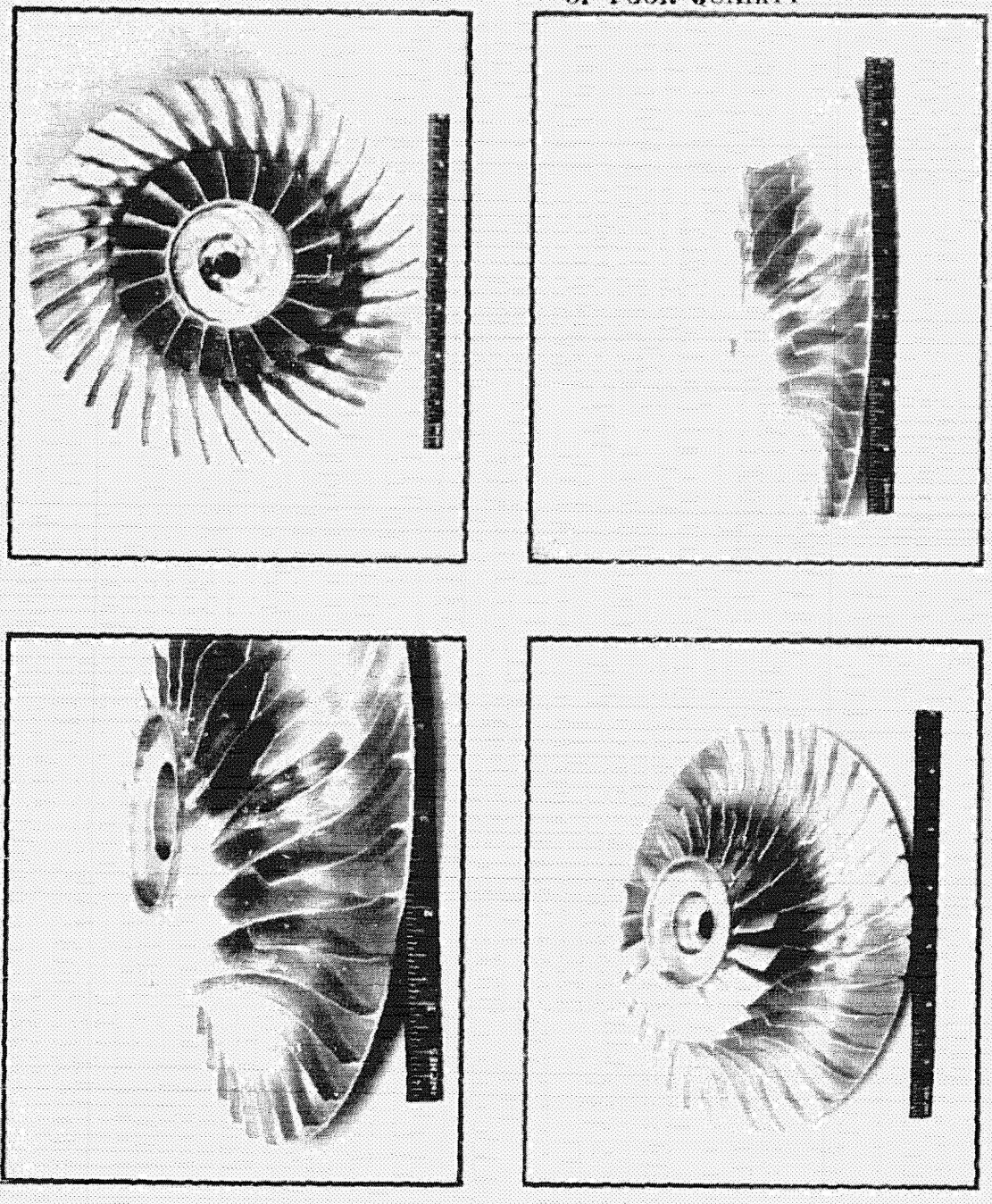

Figure 7
Front, Side and ¾ Views of 36-Blade Impeller

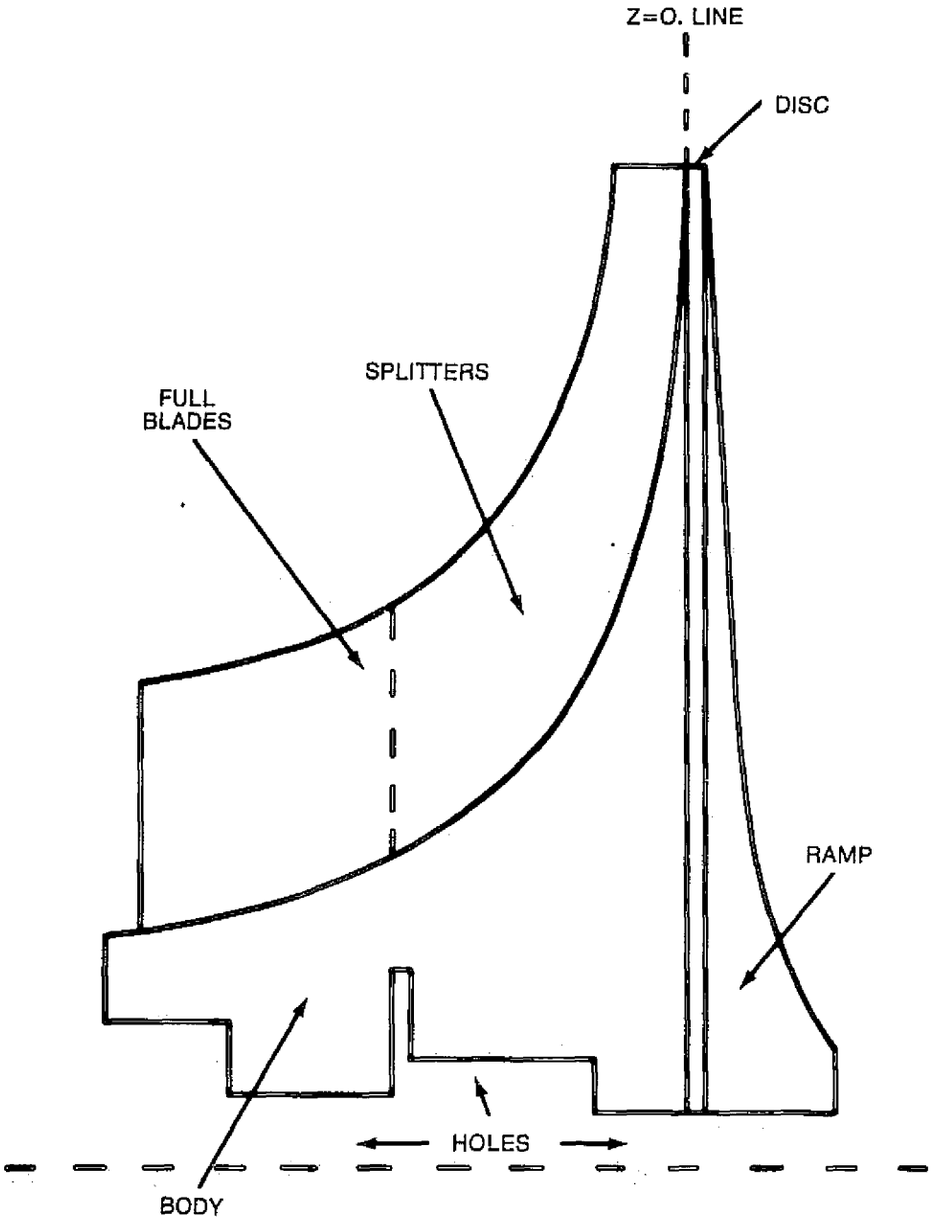

Figure 8
Breakdown of Impeller Elements
For Mass, C.G. and Inertia Calculations

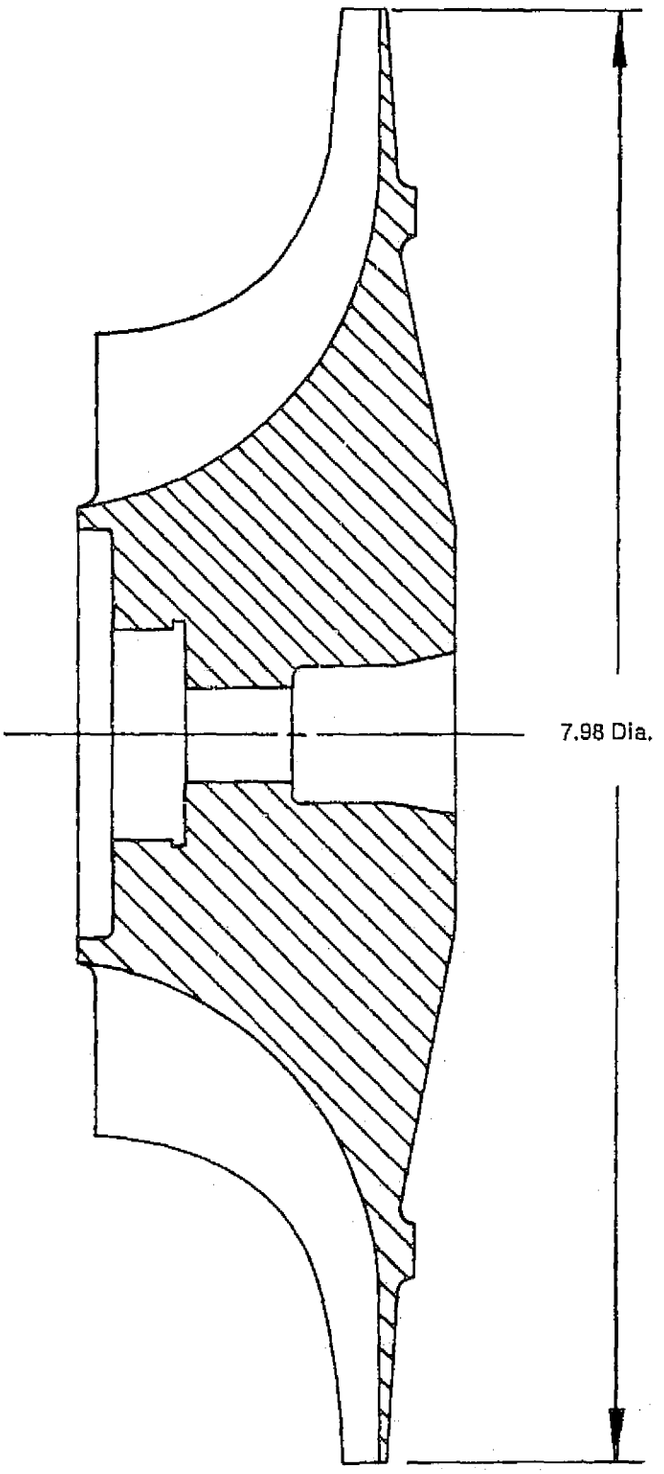

Figure 9
Impeller Configuration

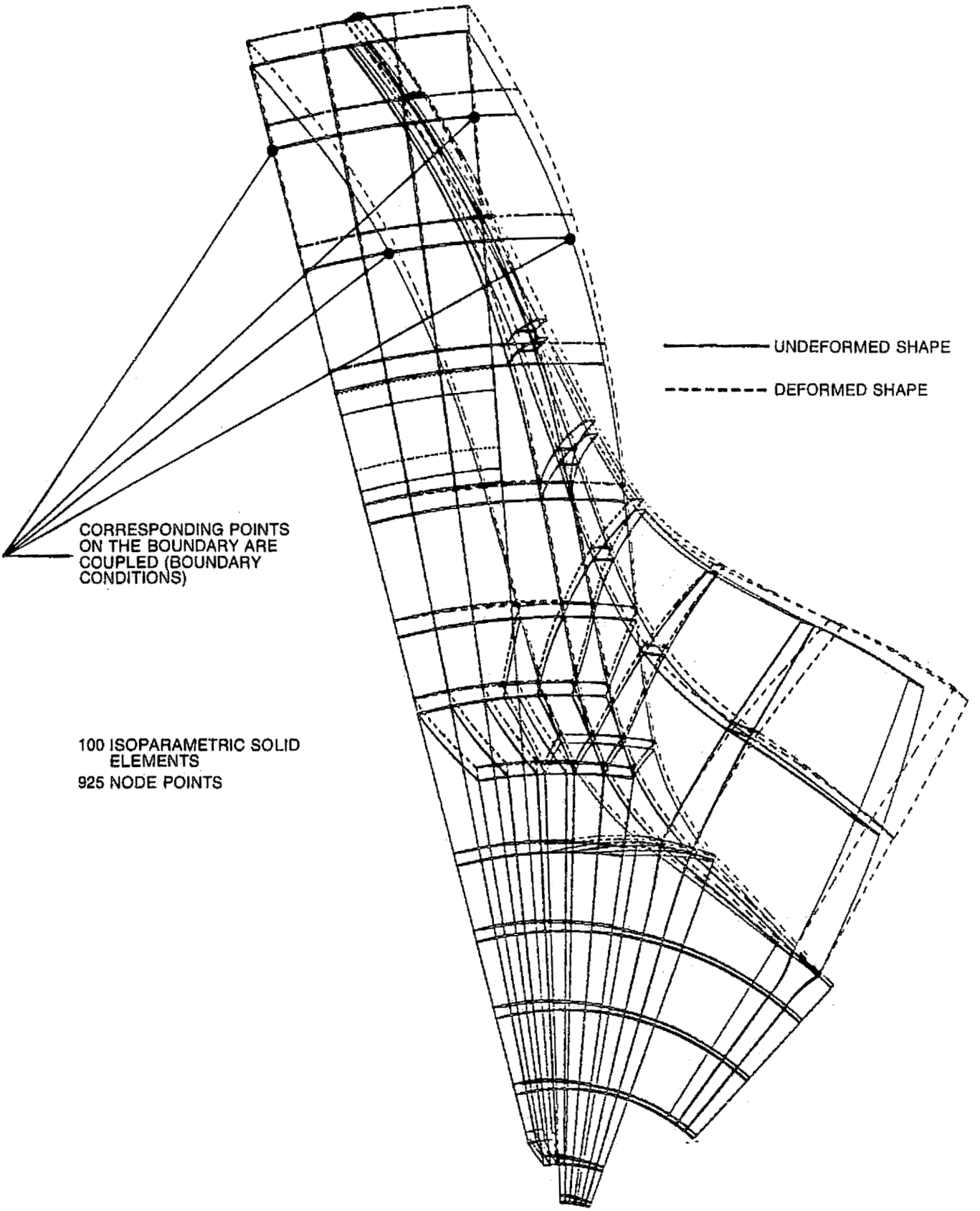

Figure 10
Finite Element Model of Impeller
10° "Spiral Wedge" Sector

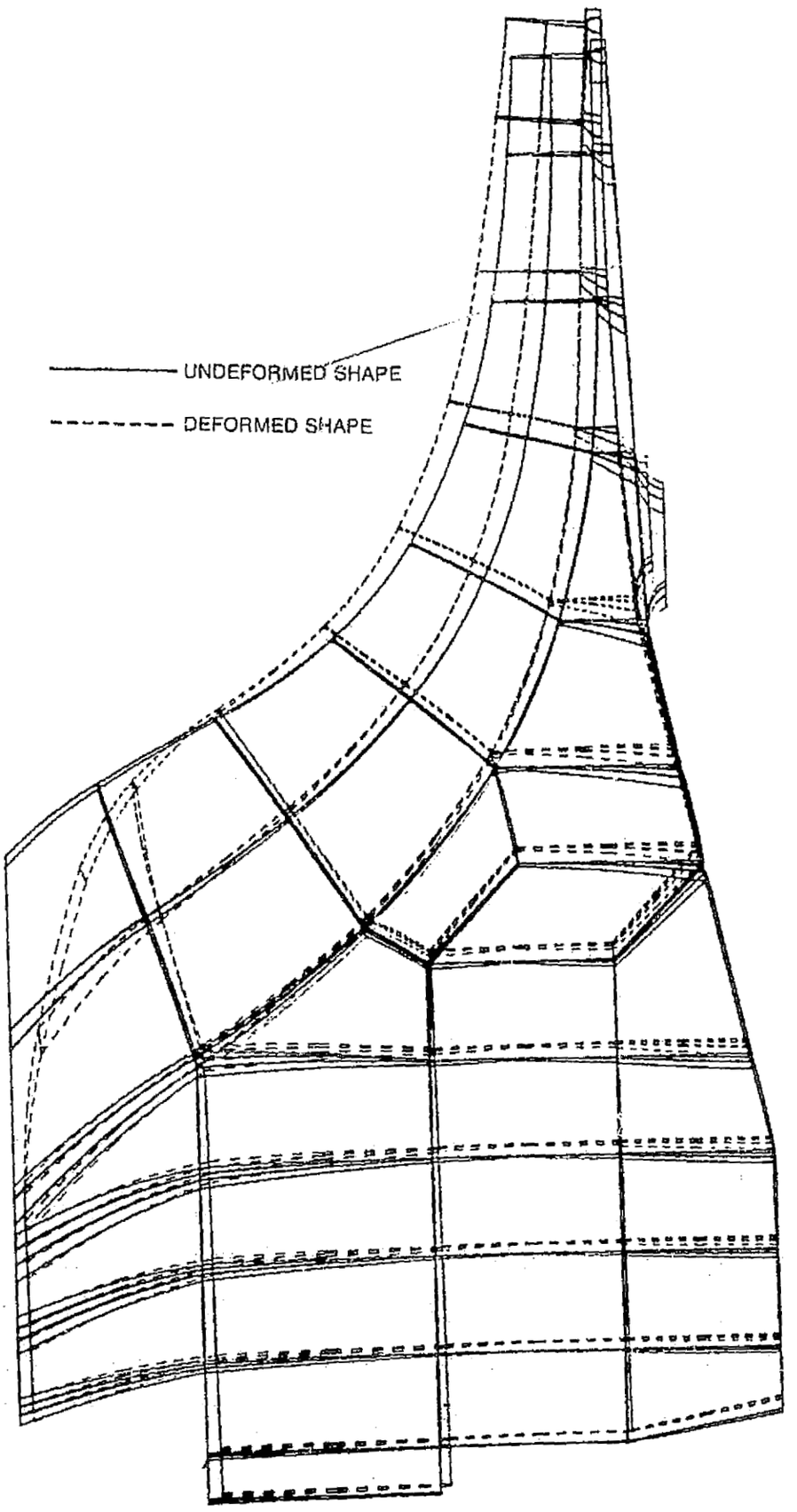

Figure 11
Meridional View
Undeformed Shape vs. Deformed Shape

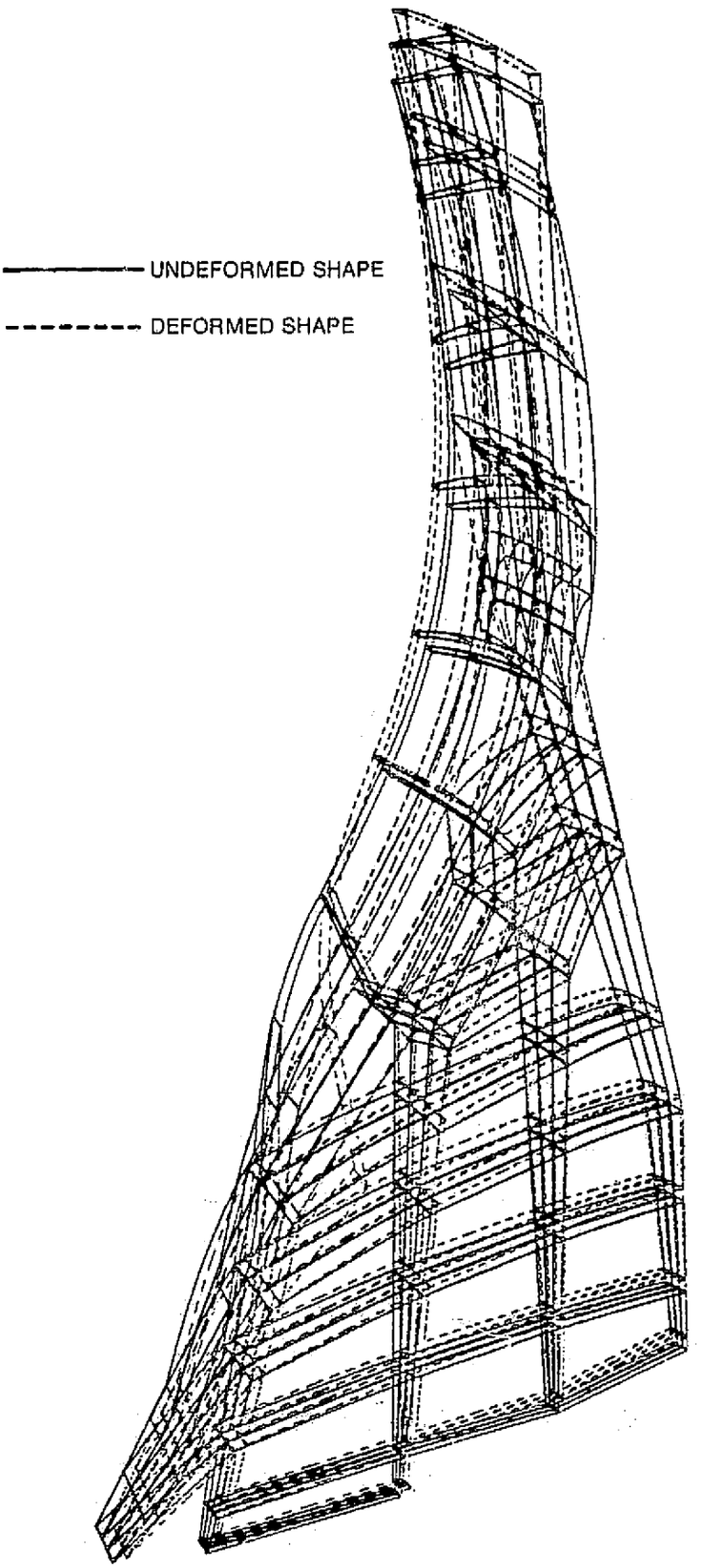

Figure 12
Oblique View
Undeformed Shape vs. Deformed Shape

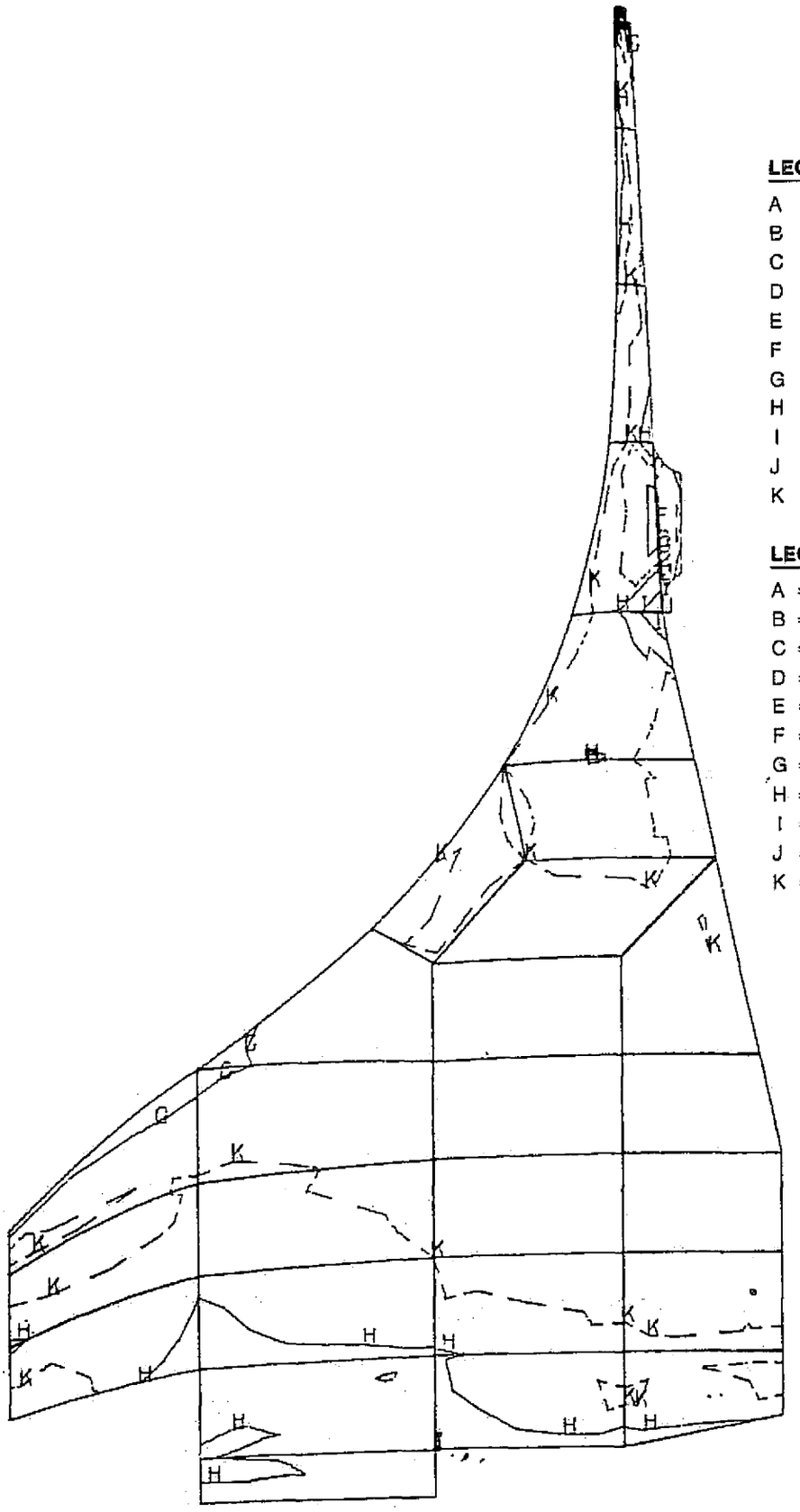

LEGEND (MPa)

A	−163.
B	−139.
C	−114.
D	− 90.
E	− 65.
F	− 41.
G	− 17.
H	8.
I	32.
J	57.
K	0.

LEGEND (PSI)

A	= −2.3677544E + 4
B	= −2.0130010E + 4
C	= −1.6582476E + 4
D	= −1.3034942E + 4
E	= −9.4874084E + 3
F	= −5.9398744E + 3
G	= −2.3923405E + 3
H	= +1.1551935E + 3
I	= +4.7027274E + 3
J	= +8.2502614E + 3
K	= 0.0000000E 0

Figure 13
Disc Principal Stress (Axial)

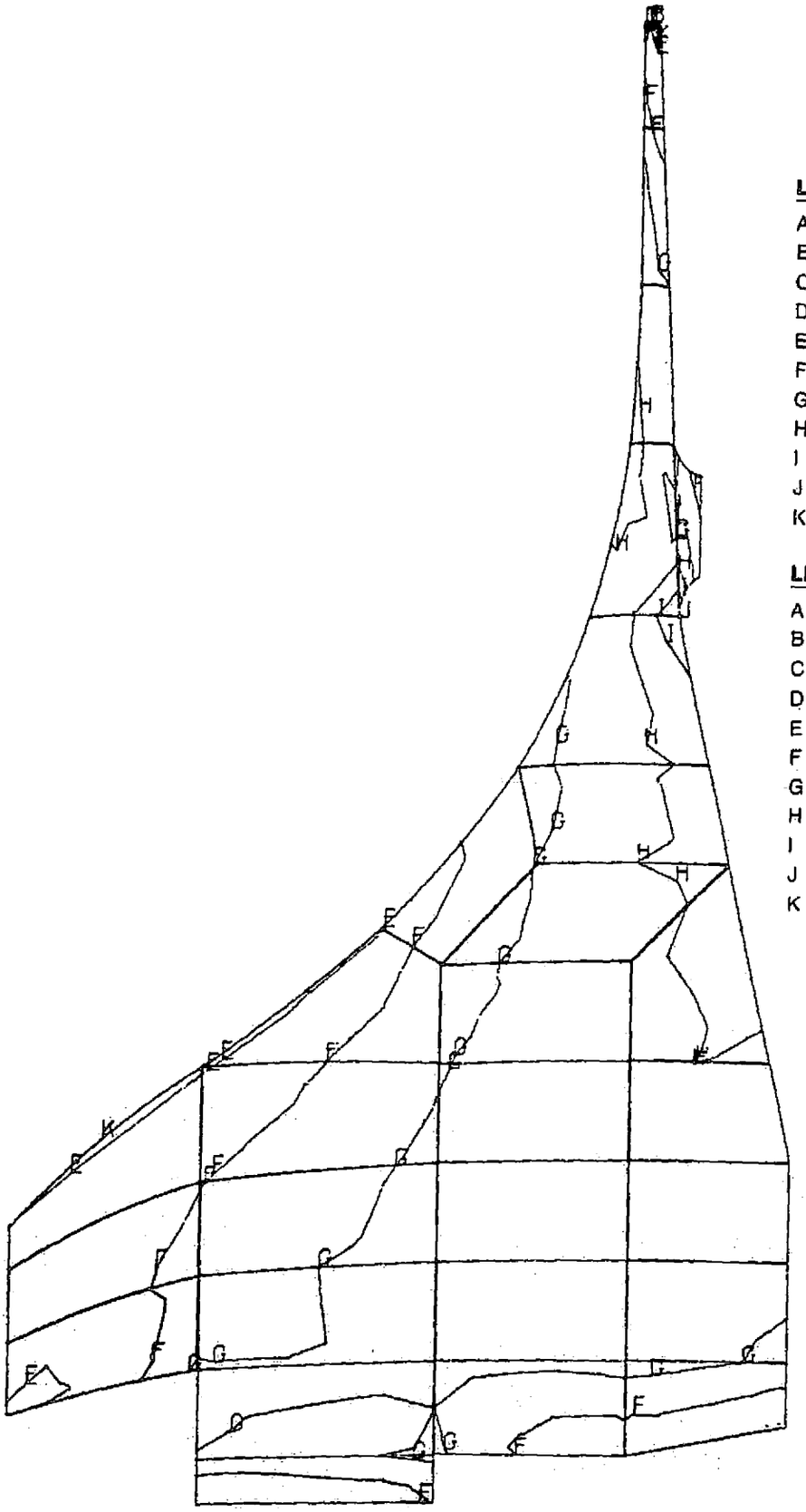

LEGEND (MPa)

A	−112.
B	− 83.
C	− 53.
D	− 24.
E	5.
F	35.
G	64.
H	94.
I	123.
J	152.
K	0.

LEGEND (PSI)

A	= −1.6293498E + 4
B	= −1.2028772E + 4
C	= −7.7640474E + 3
D	= −3.4993223E + 3
E	= +7.6540271E + 2
F	= +5.0301278E + 3
G	= +9.2948528E + 3
H	= +1.3559578E + 4
I	= +1.7824303E + 4
J	= +2.2089028E + 4
K	= 0.0000000E 0

Figure 14
Disc Principal Stress (Radial)

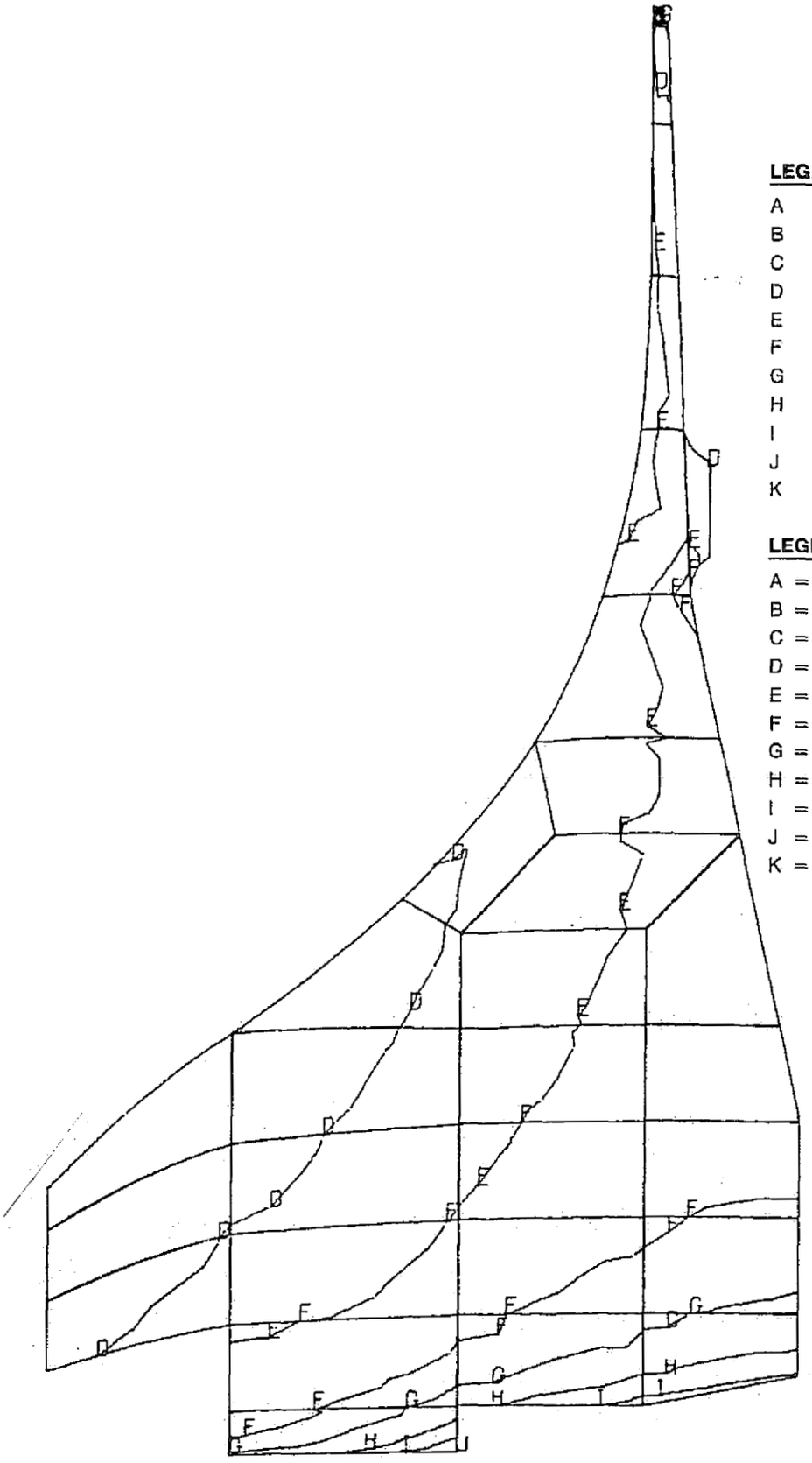

LEGEND (MPa)

A	– 27.
B	1.
C	38.
D	71.
E	103.
F	136.
G	168.
H	201.
I	234.
J	266.
K	0.

LEGEND (PSI)

A	= −3.8795017E + 3
B	= +8.4164293E + 2
C	= +5.5627876E + 3
D	= +1.0283932E + 4
E	= +1.5005077E + 4
F	= +1.9726222E + 4
G	= +2.4447366E + 4
H	= +2.9168511E + 4
I	= +3.3889655E + 4
J	= +3.8610800E + 4
K	= 0.0000000E 0

Figure 15
Disc Principal Stress (Tangential)

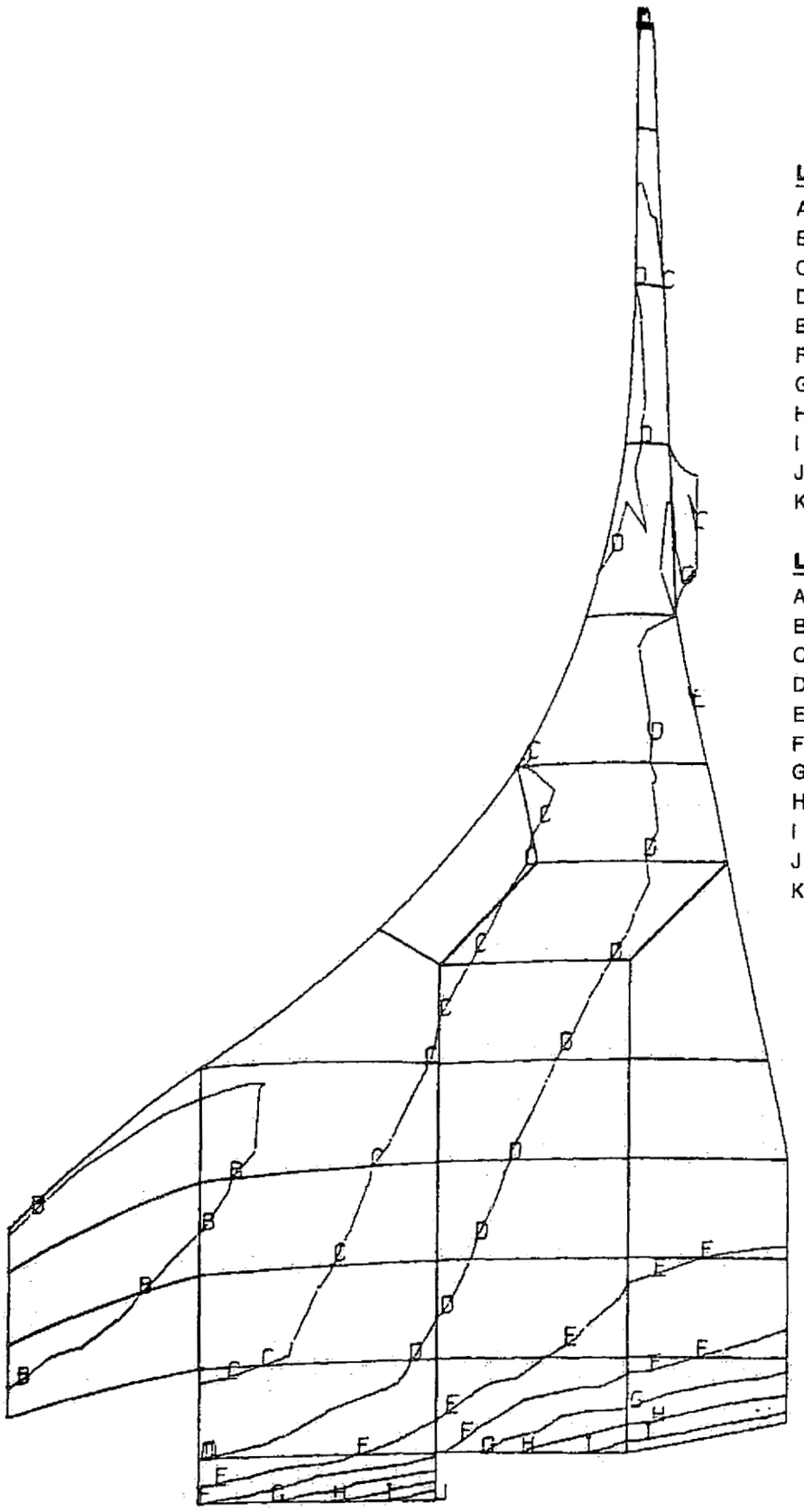

LEGEND (MPa)

A	29.
B	53.
C	76.
D	99.
E	122.
F	145.
G	168.
H	192.
I	215.
J	238.
K	0.

LEGEND (PSI)

A	= +4.2586762E + 3
B	= +7.6230621E + 3
C	= +1.0987448E + 4
D	=+1.4351834E + 4
E	= +1.7716220E + 4
F	= +2.1080606E + 4
G	= +2.4444992E + 4
H	= +2.7809378E + 4
I	= +3.1173763E + 4
J	= +3.4538149E + 4
K	= 0.0000000E 0

Figure 16
Disc Equivalent Stress

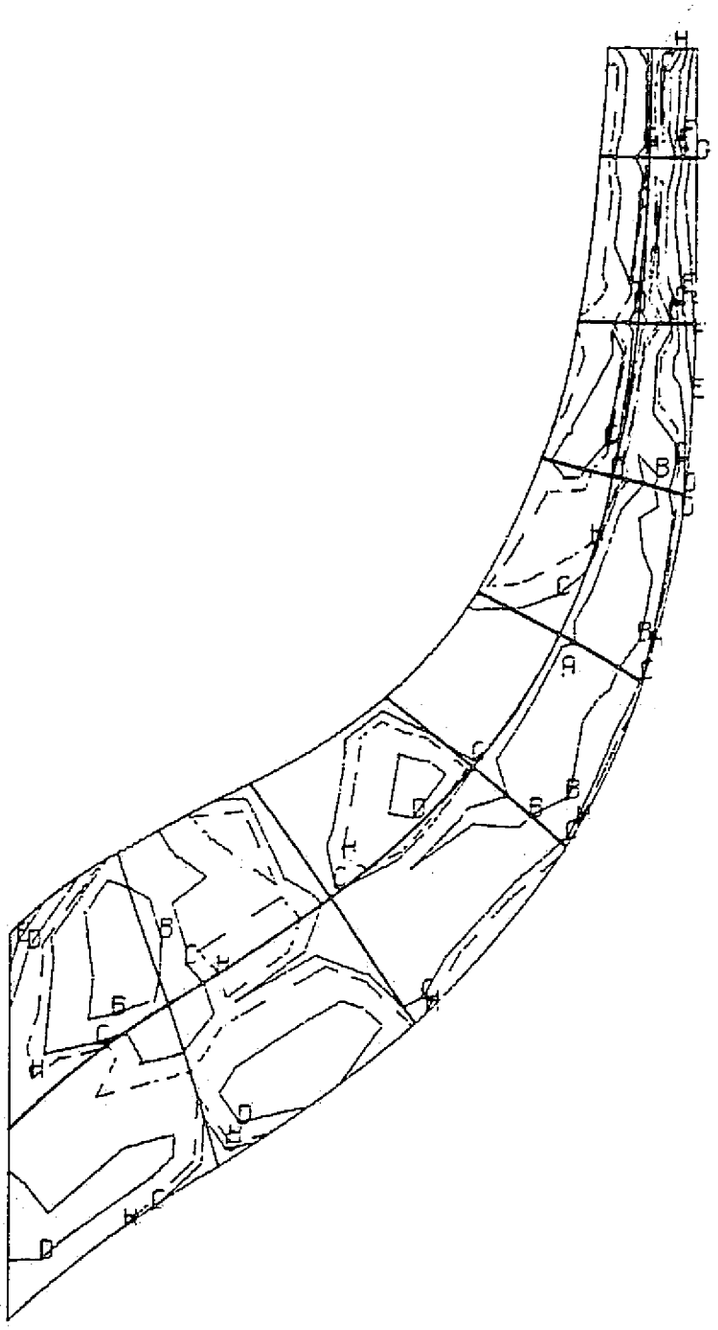

LEGEND (MPa)

A	− 23.
B	− 13.
C	− 3.
D	7.
E	17.
F	27.
G	37.
H	0.

LEGEND (PSI)

A	= −3.2609578E + 3
B	= −1.8172587E + 3
C	= −3.7355965E + 2
D	= +1.0701394E + 3
E	= +2.5138385E + 3
F	= +3.9575376E + 3
G	= +5.4012367E + 3
H	= 0.0000000E 0

Figure 17
Blade Suction Side Principal Stress #1

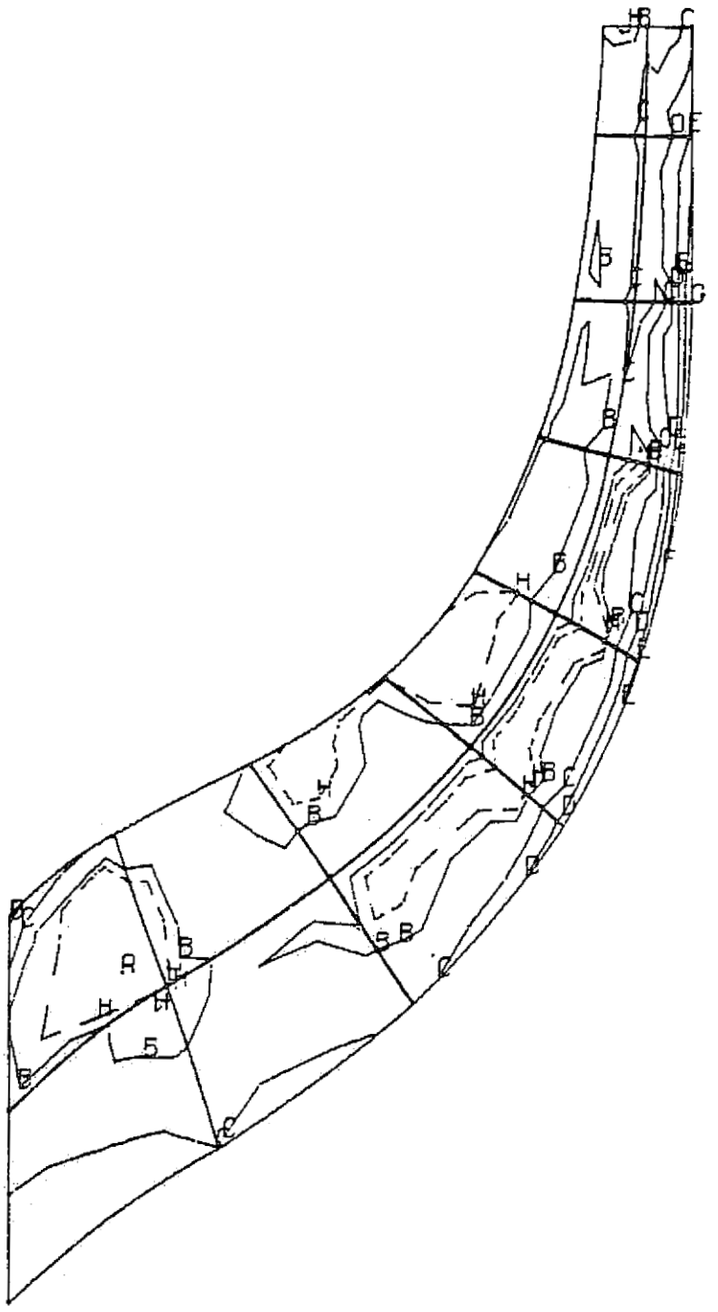

LEGEND (MPa)

A	− 14.
B	5.
C	24.
D	43.
E	63.
F	82.
G	101.
H	0.

LEGEND (PSI)

A	= −2.0046921E + 3
B	= +7.6416132E + 2
C	= +3.5330148E + 3
D	= +6.3018682E + 3
E	= +9.0707217E + 3
F	= +1.1839575E + 4
G	= +1.4608429E + 4
H	= 0.0000000E 0

Figure 18
Blade Suction Side Principal Stress #2

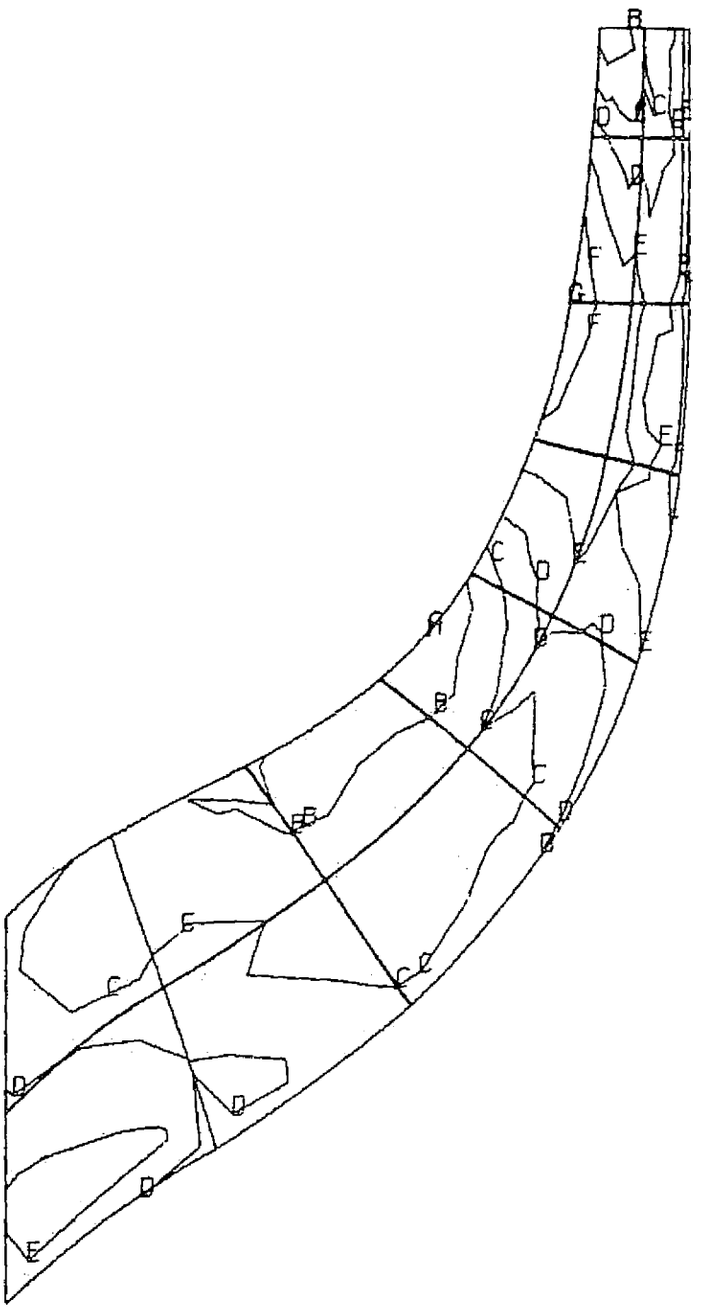

LEGEND (MPa)

A	–	.5
B		22.
C		44.
D		66.
E		88.
F		110.
G		132.
H		0.

LEGEND (PSI)

A	=	−8.1118923E + 1
B	=	+3.1215116E + 3
C	=	+6.3241421E + 3
D	=	+9.5267726E + 3
E	=	+1.2729403E + 4
F	=	+1.5932034E + 4
G	=	+1.9134664E + 4
H	=	0.0000000E 0

Figure 19
Blade Suction Side Principal Stress #3

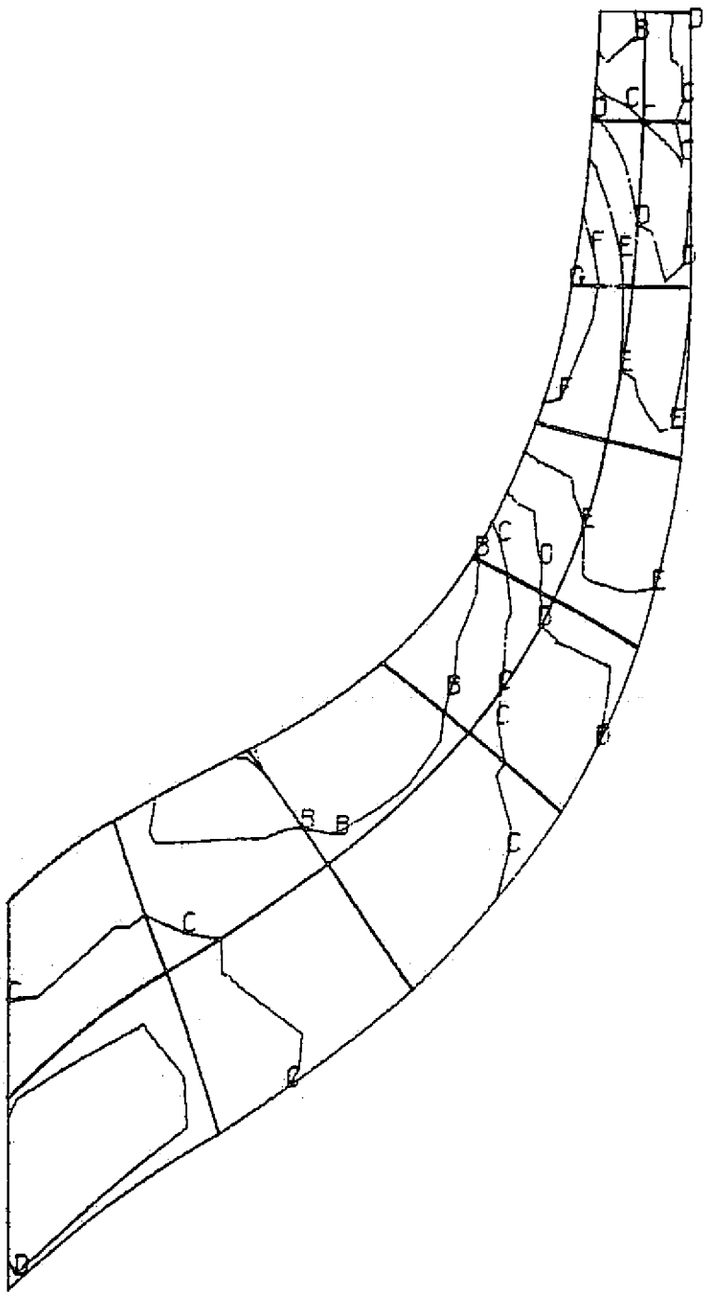

LEGEND (MPa)

A	7.
B	27.
C	47.
D	67.
E	86.
F	106.
G	126.
H	0.

LEGEND (PSI)

A	= +1.0349974E + 3
B	= +3.9108327E + 3
C	= +6.7866680E + 3
D	= +9.6625033E + 3
E	= +1.2538339E + 4
F	= +1.5414174E + 4
G	= +1.8290009E + 4
H	= 0.0000000E 0

Figure 20
Blade Suction Side Equivalent Stress

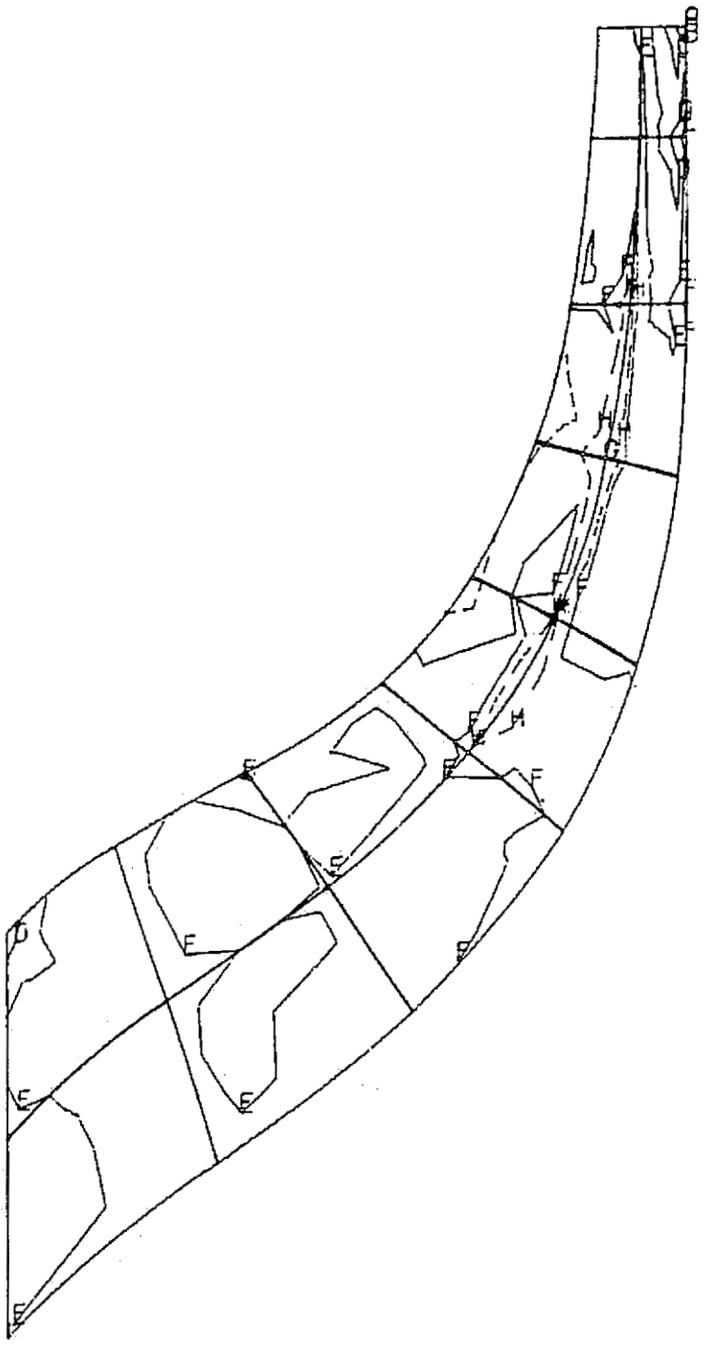

LEGEND (MPa)

A	−100.
B	− 81.
C	− 63.
D	− 44.
E	− 25.
F	− 6.
G	12.
H	0.

LEGEND (PSI)

A	= −1.4509465E + 4
B	= −1.1789530E + 4
C	= −9.0695946E + 3
D	= −6.3496595E + 3
E	= −3.6297245E + 3
F	= −9.0978943E + 2
G	= +1.8101456E + 3
H	= 0.0000000E 0

Figure 21
Blade Pressure Side Principal Stress #1

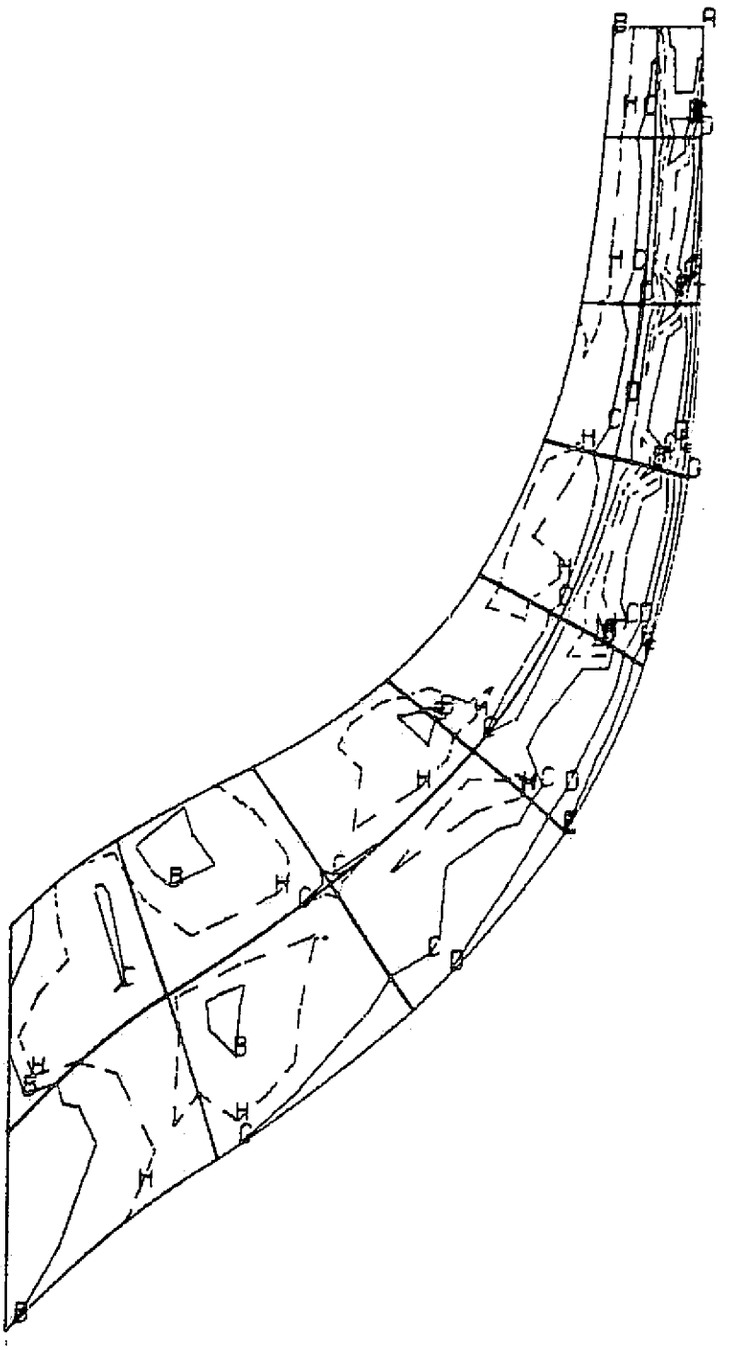

LEGEND (MPa)

A	−26.
B	− 8.
C	10.
D	28.
E	46.
F	64.
G	82.
H	0.

LEGEND (PSI)

A	= −3.7619164E + 3
B	= −1.1452456E + 3
C	= +1.4714253E + 3
D	= +4.0880961E + 3
E	= +6.7047670E + 3
F	= +9.3214378E + 3
G	= +1.1938109E + 4
H	= 0.0000000E 0

Figure 22
Blade Pressure Side Principal Stress #2

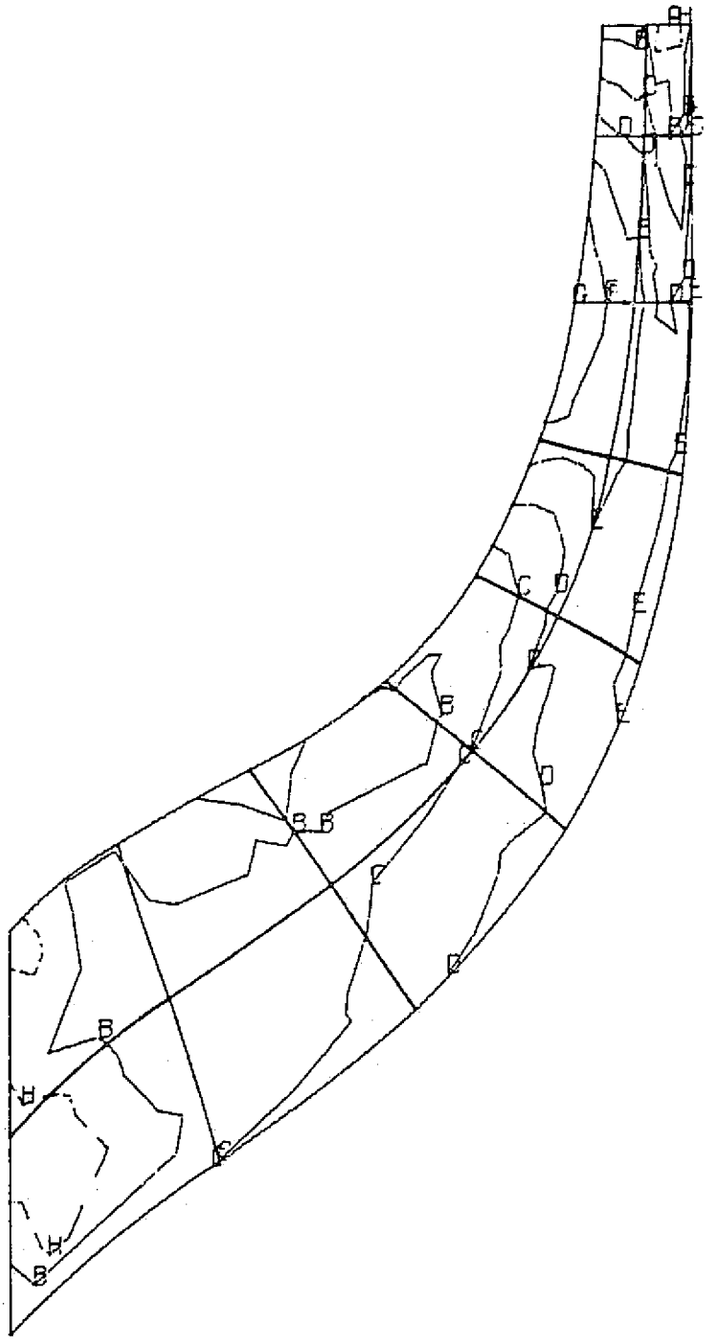

LEGEND (MPa)

A	− 12.
B	11.
C	35.
D	58.
E	81.
F	104.
G	127.
H	0.

LEGEND (PSI)

A	= −1.7165148E + 3
B	= +1.6515719E + 3
C	= +5.0196587E + 3
D	= +8.3877454E + 3
E	= +1.1755832E + 4
F	= +1.5123919E + 4
G	= +1.8492006E + 4
H	= 0.0000000E 0

Figure 23
Blade Pressure Side Principal Stress #3

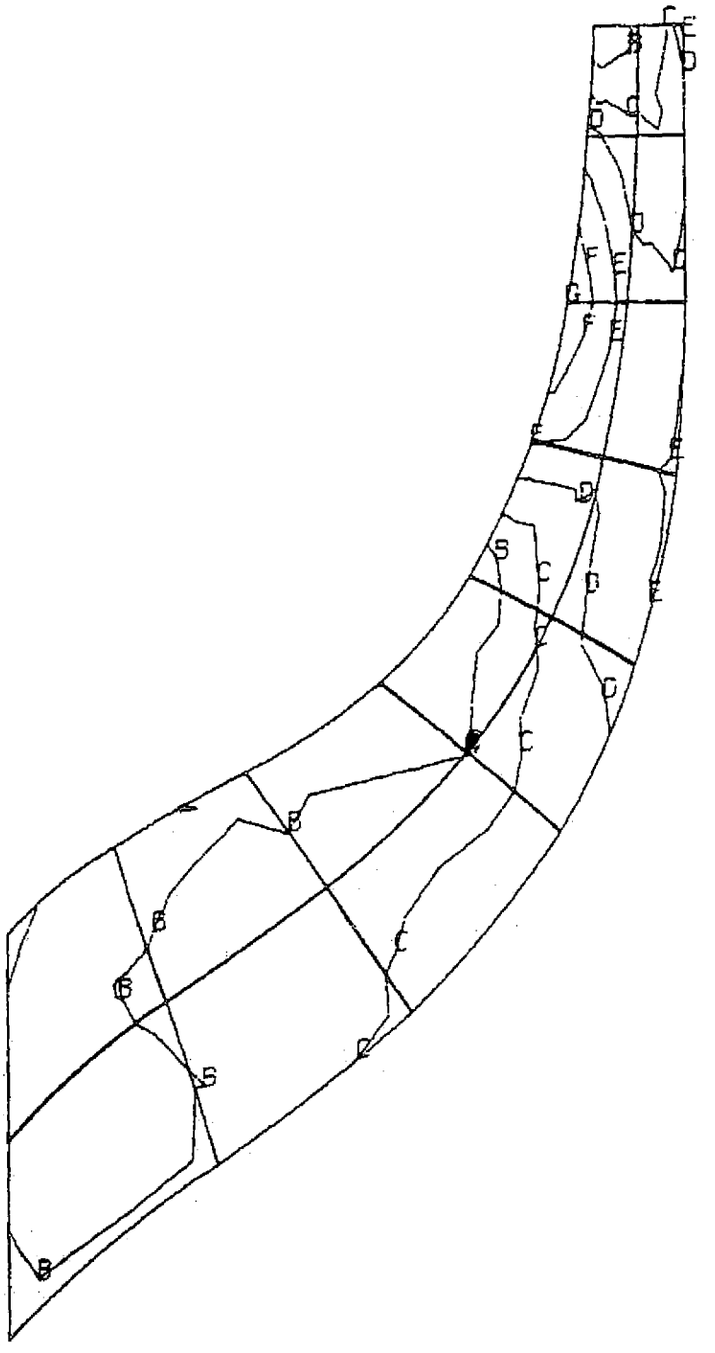

LEGEND (MPa)

A	13.
B	33.
C	53.
D	72.
E	93.
F	112.
G	132.
H	0.

LEGEND (PSI)

A	= +1.9269466E + 3
B	= +4.8009745E + 3
C	= +7.6750024E + 3
D	= +1.0549030E + 4
E	= +1.3423058E + 4
F	= +1.6297086E + 4
G	= +1.9171114E + 4
H	= 0.0000000E 0

Figure 24
Blade Pressure Side Equivalent Stress

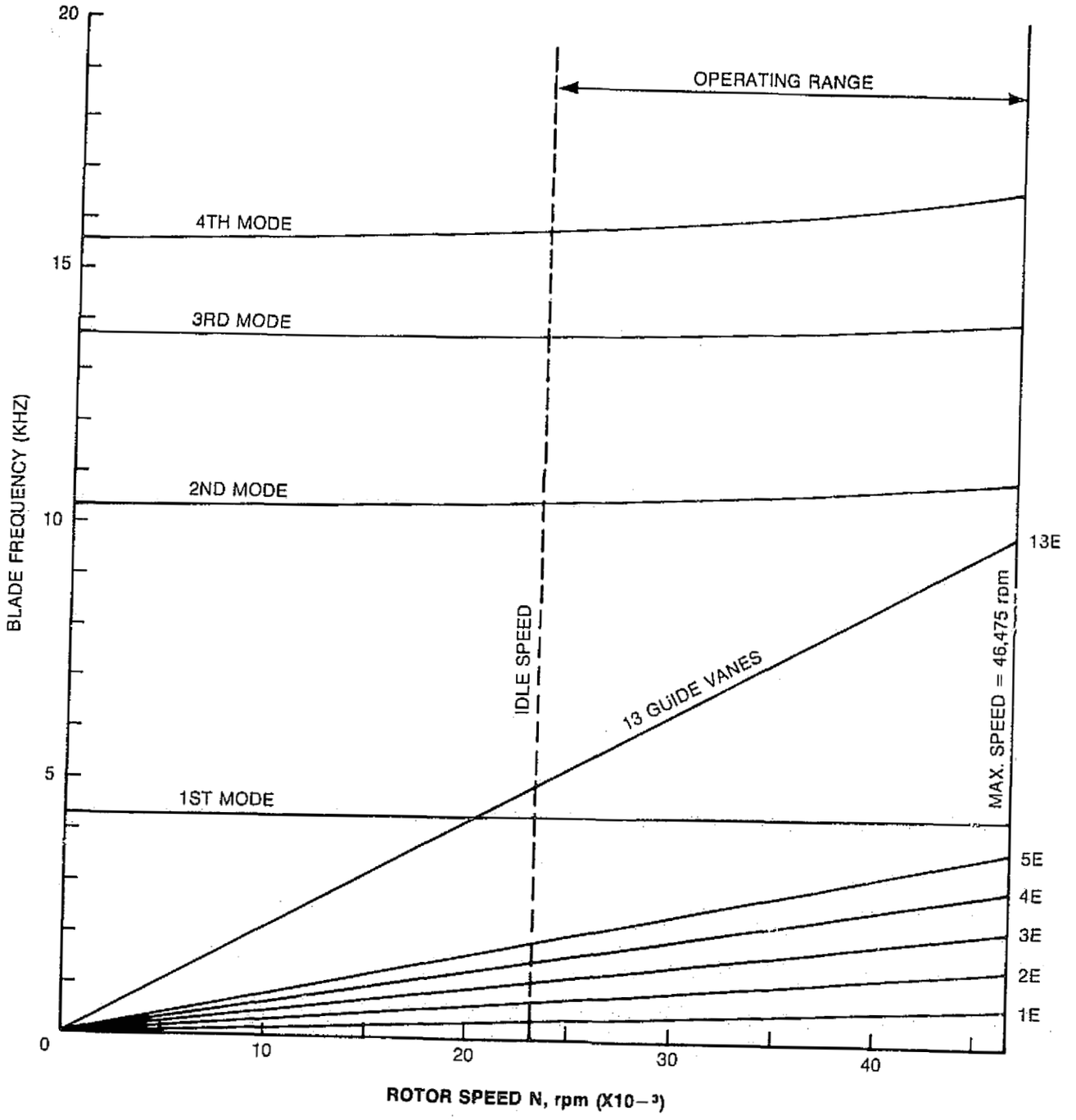

Figure 25
Impeller Campbell Diagram

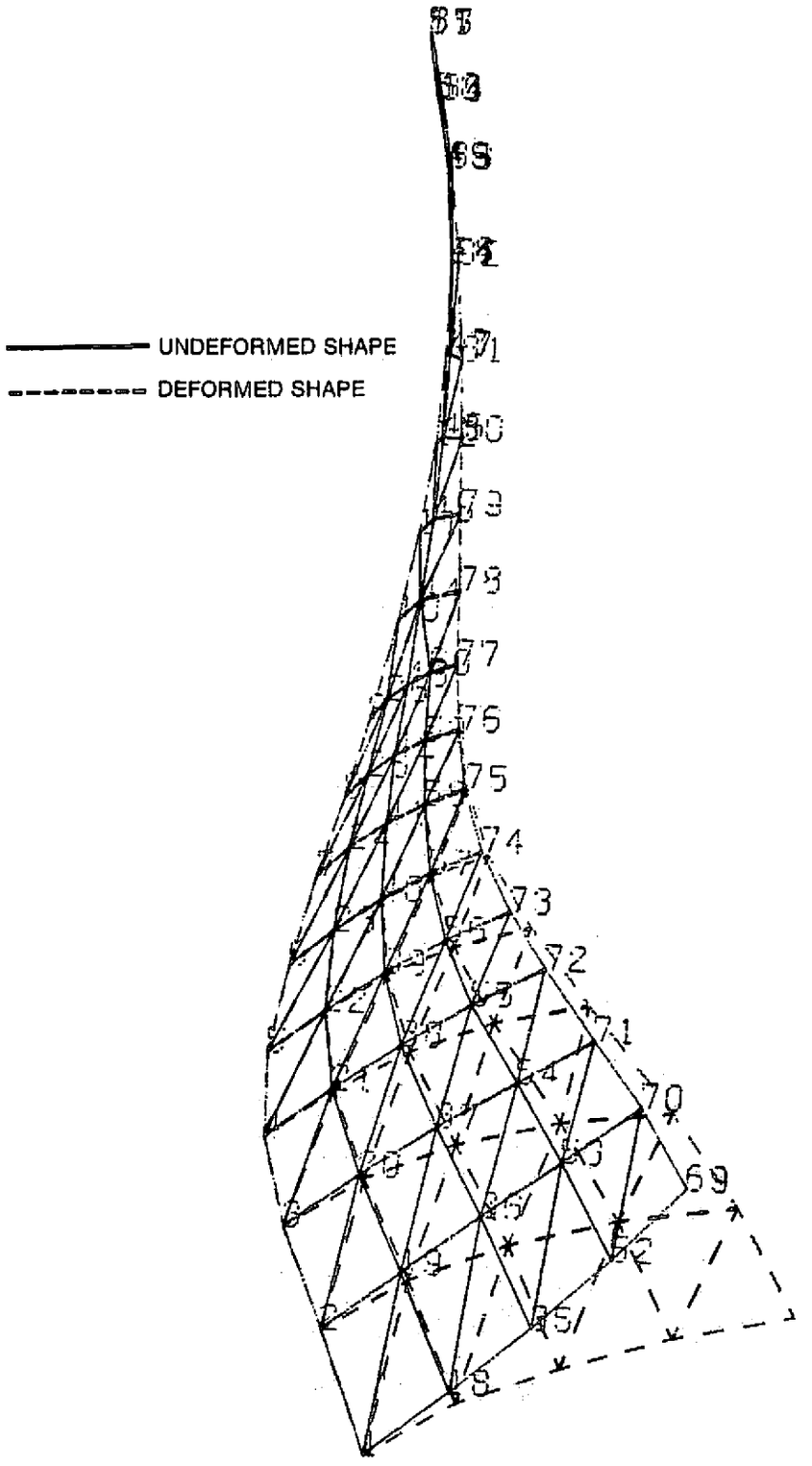

Figure 26
MODE 1 - 4317 Hz

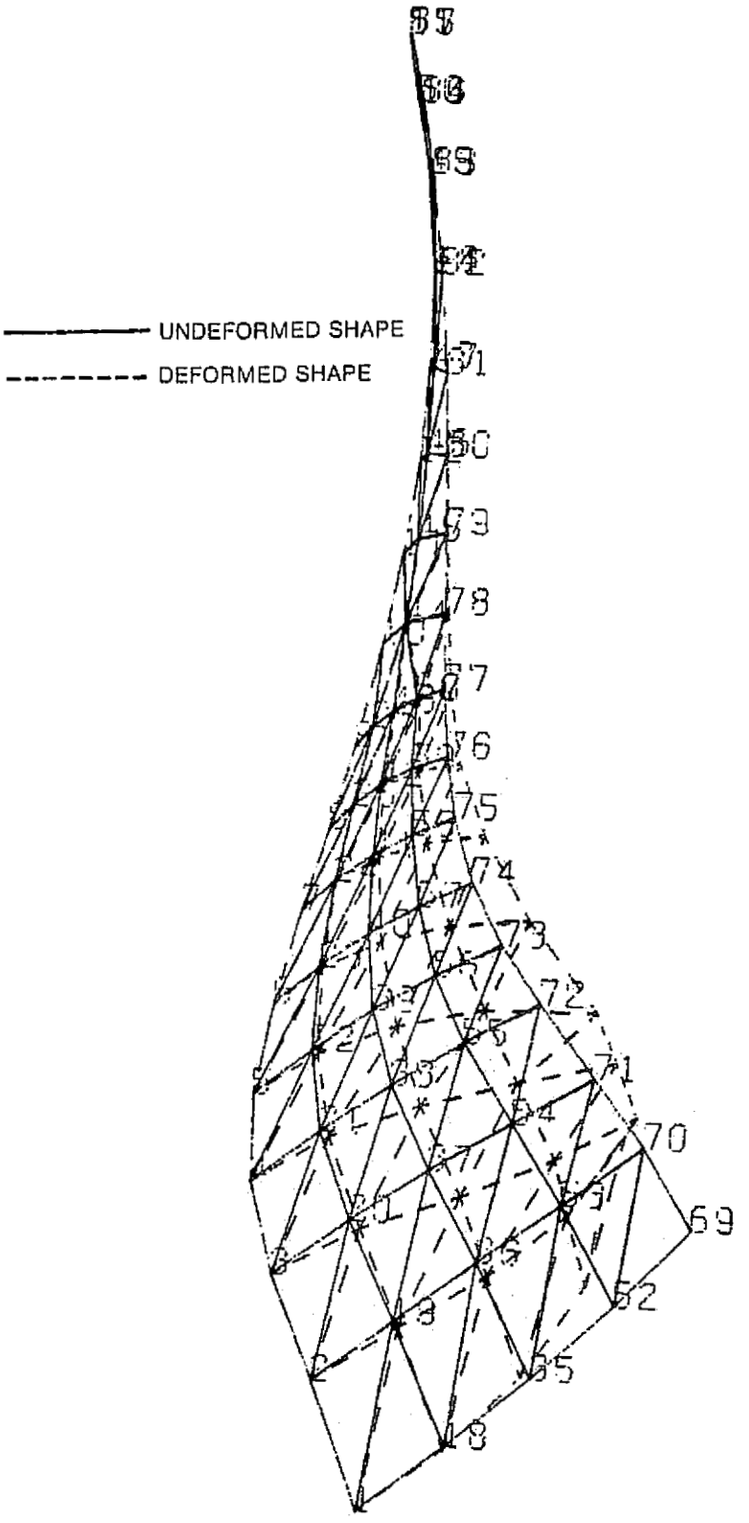

Figure 27
Mode 2 - 10, 314 Hz

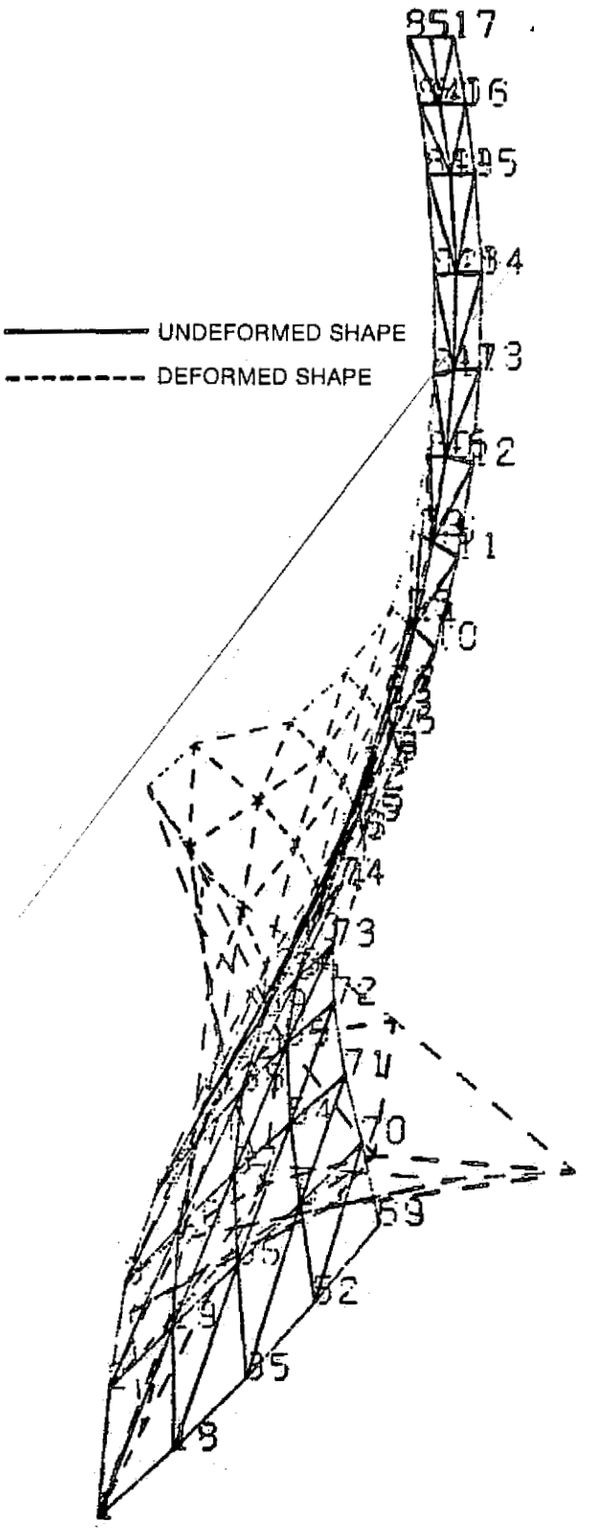

Figure 28
Mode 3 - 13,731 Hz

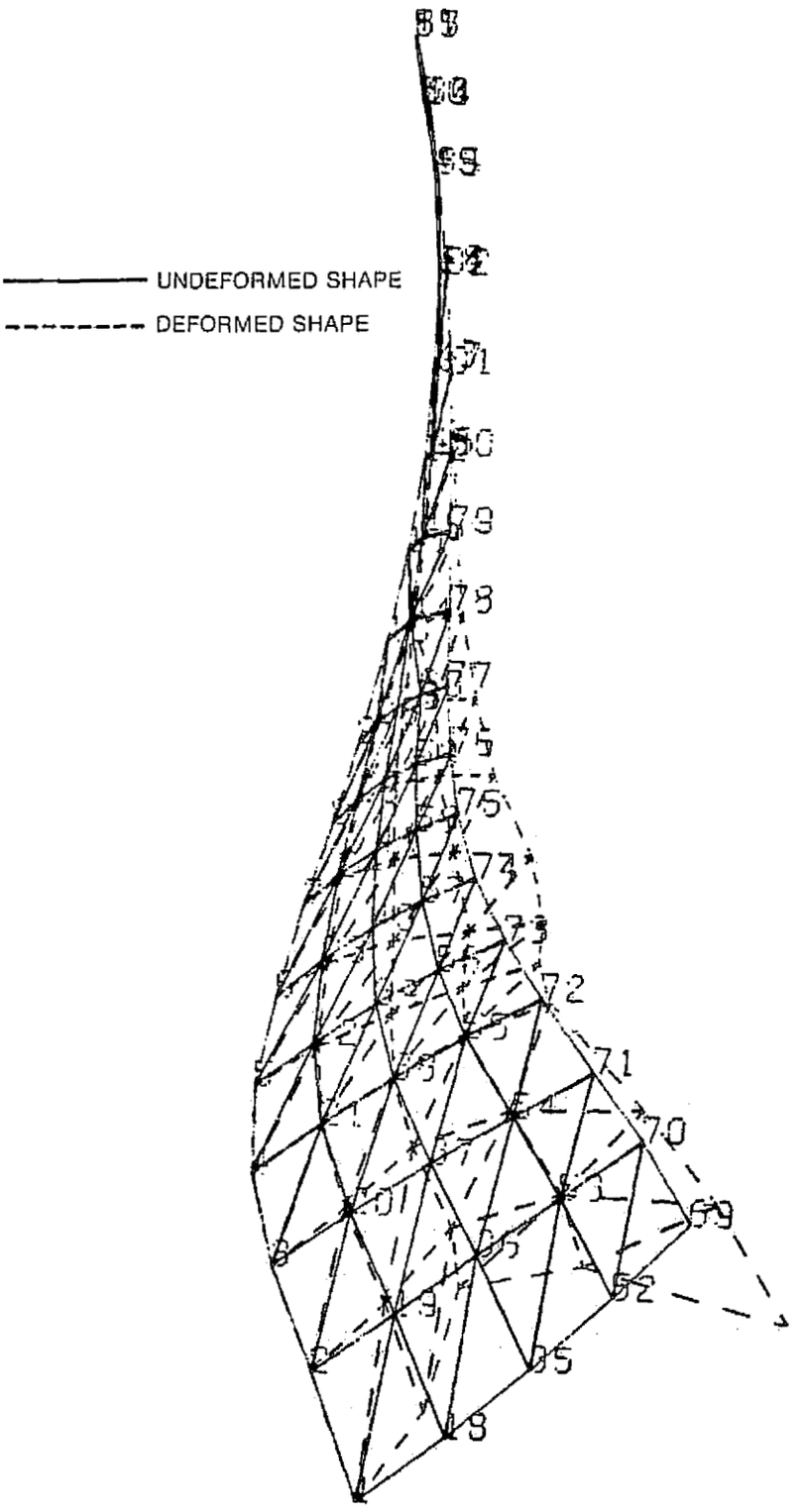

Figure 29
Mode 4-15, 616 Hz